Erickson, T.M., et al., 2019, Shock-produced high-pressure (La, Ce, Th)PO4 polymorph revealed by microstructural phase heritage of monazite: Geology, https://doi.org/10.1130/G46008.1

Item DR1: Analytical methods

Identification of Shocked Monazites and Imaging External Shock Features

Two shock-deformed crystalline samples of target rock-clast within suevitic, impact-melt bearing, breccia were investigated. Sample 604 comes from the original study of shock deformation in crystalline target rocks by Stöffler (1971) at the Nördlinger-Ries impact structure. The sample is a shock stage Ib granitic clast made up of quartz, K-feldspar, oligoclase, and biotite collected at the Otting quarry (48°52'38"N, 10°47'30"E). Quartz contains planar deformation features (PDFs) and minor stishovite, K-feldspar contain PDFs and mosaicism; oligoclase displays mosaicism and partial amorphization; and biotite contains kink bands (Stöffler, 1971; von Engelhardt et al., 1969).

The second sample, DIG 9, is derived from the Haughton Dome and is the first sample in which shock features were reported in natural monazite (Schärer and Deutsch, 1990). Sample DIG 9 was collected near the central peak of the structure (75°23'11"N, 89°38'58"W) and is a shock stage III sillimanite-biotite gneiss. Tecto-silicates (quartz, K-feldspar, plagioclase) in the gneiss are completely amorphous and vesiculated, whereas biotite has decomposed to oxides and sillimanite contains planar microstructures.

The shock stage Ib granitic sample from the Nördlinger-Ries impact structure was investigated in thin section, while monazite grains were picked from mineral separates of the shock stage III gneiss from Haughton impact structure and mounted in 25.5 mm epoxy round. The thin sections and grain mounts were given a preliminary polish to 1 μm using diamond paste. The samples were then given a final chemical-mechanical polish with 5 nm colloidal silica dispersion in NaOH on a Buehler VibroMet2 polishing machine. Grains from sampled DIG 9

and petrographic texture and grains from Nördlinger-Ries sample604 were then imaged optically.

Imaging Internal Shock Features

After polishing and optical imaging, internal textures of the deformed monazite grains were imaged using the Tescan Mira3 field emission (FE) SEM at the Microscopy & Microanalysis Facility, within the John de Laeter Centre for Isotope Research (JDLC), Curtin University, Western Australia or the JEOL 7600f FEG-SEM within the Astromaterials Research and Exploration Science (ARES) Division, NASA Johnson Space Center, Houston, Texas. Backscattered-electron (BSE) photomicrographs of the monazite grains were collected using an accelerating voltage of 15 kV. BSE photomicrographs from all shocked monazite grains are included in Data Repository Item 2.

EBSD Mapping of Monazites and Zircons

Deformed monazites were subsequently mapped by EBSD. Electron backscatter patterns (EBSPs) were collected from the monazite grains in orthogonal grids using a Nordlys Nano high resolution detector and Oxford Instruments Aztec 3.4 acquisition software package on the Mira3 FEG-SEM within the JDLC and with an Oxford Symmetry detector and Oxford Instruments Aztec 4.0 software on a JEOL 7600f FEG-SEM within ARES. EBSD analyses were collected with a 20 kV accelerating voltage, 70° sample tilt, ~20 mm working distance, and 18 nA beam current. Oxford Instruments Channel 5.11 software suite was used to post-process the EBSD data. Monazite grains were mapped with the match unit described in Erickson et al. (2016); Erickson et al. (2015), which originates from crystallographic data of Ni et al. (1995). Operating conditions and noise reduction parameters are summarized in Table DR1. EBSD maps were produced using the Tango suite of Channel5, and pole figures were processed in Mambo suite of

Channel5. EBSD maps and pole figures of the shocked monazite grains can be found in Data Repository Item DR2. Crystallographic orientation maps using all Euler color scheme with special boundary maps in which boundaries between adjacent pixels are color coded such that if they matched a specific disorientation axis and angle pair, within 5°, consistent with a twin boundary. Pole figures of (010), [100], (100), [001] and (001) were produced for each grain analyzed.

Conversion of EBSD disorientation data to deformation twins

Crystallographic orientation data obtained by EBSD can be used to calculate the misorientation between two different crystallographic orientations. This is commonly expressed as three superimposed rotations about axes specified by a convention, where the rotation angles are known as Euler angles, or a single angular rotation around a stated axis (angle-axis pair). Depending on the crystal symmetry there may be more than one angle-axis pair that achieves the same rotation but the rotation angles will be different. The disorientation convention used in this paper means that the angle-axis pair with the smallest angular rotation is chosen from all the symmetrically equivalent rotations. For monoclinic minerals, of which monazite is one, there are only two symmetric equivalents. This arises from the diad axis of symmetry parallel to the [010] direction and the fact that EBSD data can only describe proper rotations (i.e., the mirror plane perpendicular to [010] is not a proper rotation).

While the disorientation can be used to document twin microstructures, it is often cryptic and not geometrically meaningful. The relationship between two parts of a twin can be described by one (or both) of two 180° rotations that are geometrically related to either the composition plane, (K1) or shear direction(η1) (summarized in Figure DR1 after Christian and Mahajan (1995). For type 1 twins, the twin is related to the host by a 180° rotation around the pole to (a

rational) K1. For type 2 twins, the twin is related to the host by a 180° rotation around (a rational) η1. Composite twins satisfy both constraints.

To document the nature of the twins observed in monazite and identify the composition planes, pairs of Euler angles from twin and host were used to calculate not only the disorientation axis but also the hypothetical orientations of its symmetrical equivalent variants. In each case, except one, the misorientation calculation revealed a 180° rotation that was not always apparent from the disorientation. Where the 180° rotation axis was close to a pole to a rational plane this was noted to be a type 1 twin relationship and where it was close to a rational crystallographic direction the twin was documented as a type 2 relationship. Several twins (those with a disorientation rotation of 180°) satisfied both of these criteria and were determined to be composite twins. The procedure was implemented in Matlab using the unit cell parameters of natural monazite after Ni et al. (1995) as follows:

1. Constructs a list of directions and planes in the crystal reference frame, removing collinear ones (e.g. 111 and 222).
2. Calculates the x,y,z orientation of each of the directions and plane normal for a crystal with Euler angles (0 0 0). This takes into account the crystal unit cell parameters.
3. Calculate the symmetry operators (Si) for the Laue group. In this case there are only 2 symmetrical equivalents which are related by a 180° rotation around [0 1 0].
4. For each pair of sets of Euler angles do the following:
    a. Calculate the rotation matrix (DCM) for each Euler angle triple using equations B2 and B4 of Cho et al. (2005).
    b. Calculate the rotation from one to the other (DCM3 = DCM2 – DCM1).

c. Calculate the rotation matrix for each symmetric equivalent (DCM3i = Si x DCM3).

d. Calculate the angle and axis (in Cartesian x,y,z coordinates) of rotation for each resulting rotation matrix.

e. Calculate the crystallographic index of each rotation axis. This approach gives the closest zone axis. It should be noted that where the rotation axis is a pole to a plane then it is not necessarily a rational direction (especially in monoclinic minerals where only (010)=[010]).

f. For a list of planes from where {h, k, l} are integers from -3 to 3 calculate the angle in x,y,z co-ordinates between the rotation axis and the plane normal (using dot product of unit vectors). If the angle is >90° then use the supplementary angle to thereby ignore polarity of the poles to planes; i.e., (001) = (00-1).

g. Compile the data into an output format giving the angle and axis (in x,y,z) for each symmetric variant, crystallographic vector (with smallest value normalized to 1), angle between rotation axis and closest direction, and angle between rotation axis and closest pole to plane.

The input parameters and results of the script are summarized in DR3.

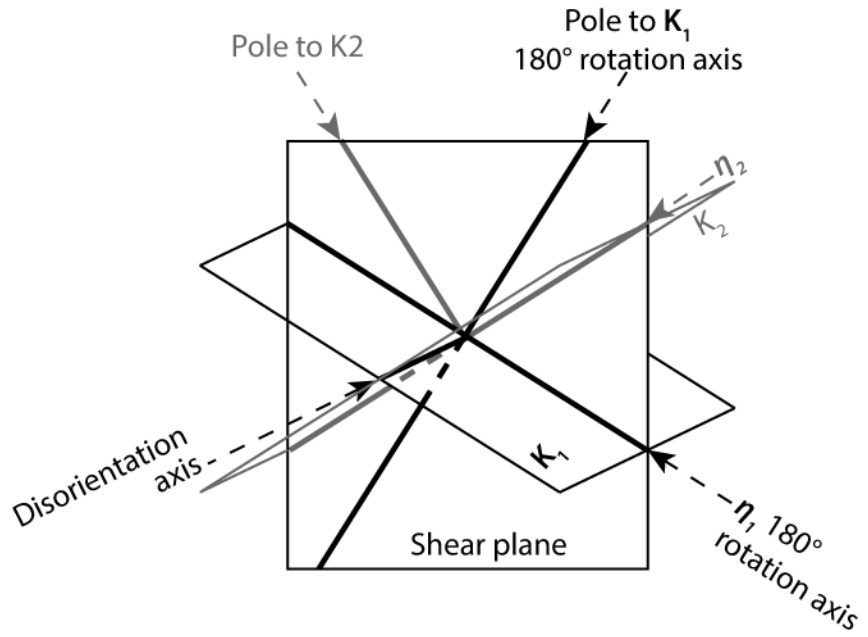

Figure DR1. Twin mode conventions modified after Christian and Mahjan (1995)

Conversion of EBSD data to high pressure polymorph orientations

The Python-based software combination of ARPGE (Cayron, 2007a) and GenOVa (Cayron, 2007b) were used to perform a crystallographic orientation analysis of monazite (monoclinic $REEPO_4$) to reconstruct evidence for precursor tetragonal $REEPO_4$ following the approach applied by Cayron et al. (2006), utilized for understanding the behavior of steels (e.g., the martensite-austenite transformation) and zirconia (Timms et al., 2017; White et al., 2018). To back-calculate the transformation mechanism of the lath-like microstructure to a high-pressure polymorph, the following steps were taken:

1. Analysis of the EBSD map and pole figures to determine the orientation relationship (OR) between the (hypothetical) parent tetragonal phase and the daughter monazite daughter phase.
2. Create the phase transformation with GenOVa to simulate the theoretical pole figures and calculate the groupoid composition table.

3. Use ARPGE to reconstruct the parent tetragonal phase from the EBSD maps and the OR determined at step 2.

This method automatically and objectively reconstructs ‘parent’ grains using known sets of orientation relationships among ‘daughter’ grains. While no preexisting constraints on the crystal structure of the high-pressure parent $REEPO_4$ phase exist, we based the tetragonal parent on the geometric distribution of the reverted daughter products. The lattice parameters used for the phases are a = b = 6.5 Å and c = 7.0 Å for the tetragonal phase, and a=6.7902 Å, b = 7.0203 Å, c = 6.4674 Å, ans $\beta = 103.4°$ for the monoclinic phase.

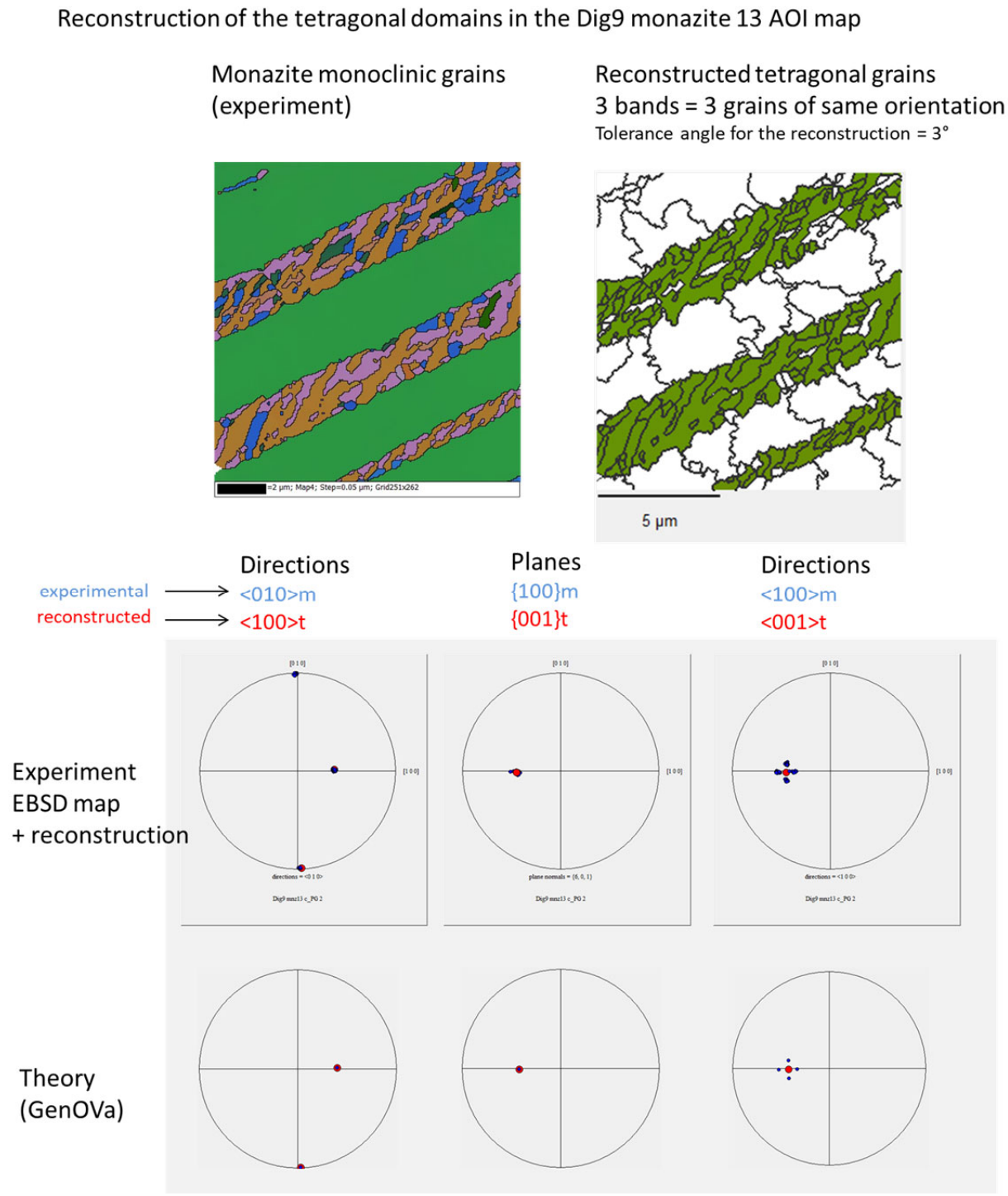

Figure DR2. Reconstruction of tetragonal parent grain from EBSD data and produced pole figures and maps using GenOVa (theoretical) and ARPGE (from data) python programs.

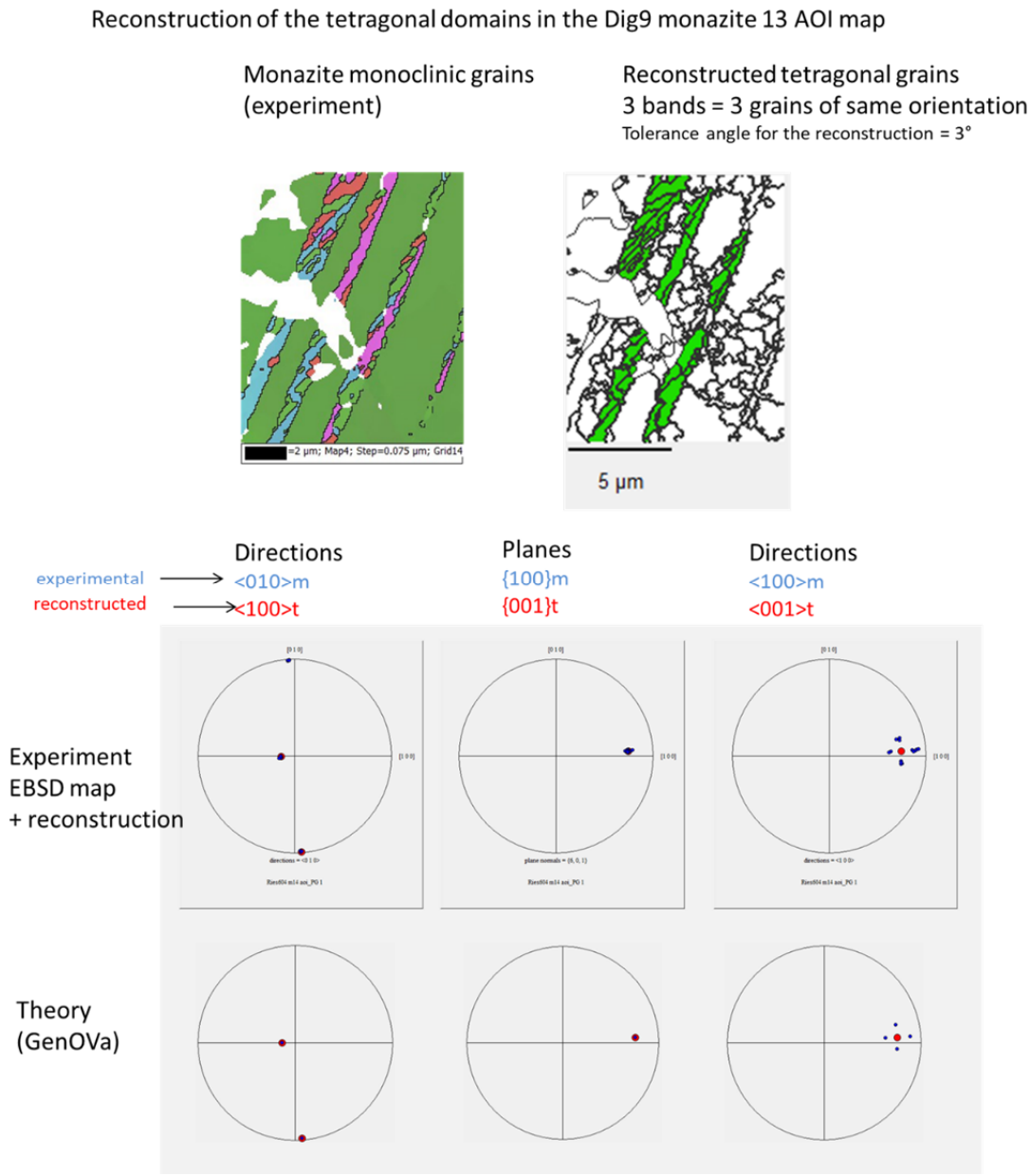

Figure DR3 Reconstruction of tetragonal parent grain from EBSD data and produced pole figures and maps using GenOVa (theoretical) and ARPGE (from data) python programs.

Table DR1.1 EBSD analytical conditions for sample Ries 604 grains 13 & 14

Figure	Ries 604 13 wholegrain	Ries 604 13 AOI 1	Ries 604 14 wholegrain	Ries 604 14 AOI 1
Acquisition speed (Hz)	40	40	40	40
Background (frames)	64	64	64	64
Binning	4x4	4x4	4x4	4x4
Gain	High	High	High	High
Hough resolution	60	60	60	60
Band detection min/max	6/8	6/8	6/8	6/8
Mean angular deviation	0.3919	0.4527	0.5216	0.5363
X steps	320	141	868	270
Y steps	225	172	1696	135
Step distance (μm)	0.2	0.075	0.07	0.05
Noise reduction – 'wildspike'	Yes	No	No	No
n neighbour zero solution extrapolation	7	7	7	7
Kuwahara Filter	-	-	-	-
SEM model	Tescan	Tescan	Tescan	Tescan
EBSD detector	Nordlys	Nordlys	Nordlys	Nordlys
Acquistion software (Aztec v.)	3.4	3.4	3.4	3.4
Carbon coat (<5nm)	Yes	Yes	Yes	Yes
Acc. Voltage (kV)	20	20	20	20
Working distance (mm)	20	20	20	20
Tilt (degrees)	70	70	70	70

Table DR1.2 EBSD analytical conditions sample DIG 9 grains 4, 5

Figure	DIG 9 grain 4 wholegrain	DIG 9 grain 4 AOI 1	DIG 9 grain 4 AOI2	DIG 9 grain 5 wholegrain	DIG 9 grain 5 AOI1
Acquisition speed (Hz)	70	40	40	322	298
Background (frames)	64	64	64	64	64
Binning	2x2	4x4	4x4	4x4	4x4
Gain	High	High	High	High	High
Hough resolution	60	60	60	60	60
Band detection min/max	6/11	6/8	6/8	6/11	6/11
Mean angular deviation	1.007	0.3985	0.4509	1.032	1.012
X steps	1109	230	221	950	631
Y steps	1278	214	132	843	528
Step distance (µm)	0.2	0.1	0.15	0.2	0.1
Noise reduction – 'wildspike'	Yes	Yes	Yes	Yes	Yes
n neighbour 0 solution extrapolation	7	7	7	7	7
Kuwahara Filter	-	-	-	-	-
SEM model	JEOL	Tescan	Tescan	JEOL	JEOL
EBSD detector	Symmetry	Nordlys	Nordlys	Symmetry	Symmetry
Acquistion software (Aztec v.)	4.0	3.4	3.4	4.0	4.0
Carbon coat (<5nm)	Yes	Yes	Yes	Yes	Yes
Acc. Voltage (kV)	20	20	20	20	20
Working distance (mm)	20	20	20	20	20
Tilt (degrees)	70	70	70	70	70

Table DR1.3 EBSD analytical conditions sample DIG 9 grains 12, 13 & 30

Figure	DIG 9 grain 12 AOI 1	DIG 9 grain 13 wholegrain	DIG 9 grain 13 AOI1	DIG 9 grain 30 wholegrain	DIG 9 grain 30 AOI1
Acquisition speed (Hz)	40	166	40	134	134
Background (frames)	64	64	64	64	64
Binning	4x4	4x4	4x4	4x4	4x4
Gain	High	High	High	High	High
Hough resolution	60	60	60	60	60
Band detection min/max	6/8	6/11	6/8	6/11	6/11
Mean angular deviation	0.3576	0.7758	0.3488	0.7749	0.7652
X steps	180	3117	251	298	316
Y steps	169	1946	262	234	337
Step distance (µm)	0.3	0.2	0.05	0.5	0.25
Noise reduction – 'wildspike'	Yes	Yes	Yes	Yes	Yes
n neighbour 0 solution extrapolation	7	7	7	7	7
Kuwahara Filter	-	-	-	-	-
SEM model	Tescan	JEOL	Tescan	JEOL	JEOL
EBSD detector	Nordlys	Symmetry	Nordlys	Symmetry	Symmetry
Acquistion software (Aztec v.)	3.4	4.0	3.4	4.0	4.0
Carbon coat (<5nm)	Yes	Yes	Yes	Yes	Yes
Acc. Voltage (kV)	20	20	20	20	20
Working distance (mm)	20	20	20	20	20
Tilt (degrees)	70	70	70	70	70

Table DR1.4 EBSD analytical conditions sample DIG 9 grains 32, 33

Figure	DIG 9 grain 32 wholegrain	Dig 9 grain 32 AOI 1	DIG 9 grain 32 AOI 2	DIG 9 grain 33 wholegrain	DIG 9 grain 33 AOI1	DIG 9 grain 33 AOI2
Acquisition speed (Hz)	305	303	303	305	305	306
Background (frames)	64	64	64	64	64	64
Binning	4x4	4x4	4x4	4x4	4x4	4x4
Gain	High	High	High	High	High	High
Hough resolution	60	60	60	60	60	60
Band detection min/max	6/11	6/11	6/11	6/11	6/11	6/11
Mean angular deviation	1.035	1.038	0.9978	1.053	1.06	1.072
X steps	624	510	563	541	779	550
Y steps	749	470	346	515	627	334
Step distance (µm)	0. 2	0.1	0.1	0.2	0.1	0.05
Noise reduction – 'wildspike'	Yes		Yes	Yes	Yes	Yes
n neighbour 0 solution extrapolation	7		7	7	7	7
Kuwahara Filter	-		-	-	-	-
SEM model	JEOL	JEOL	JEOL	JEOL	JEOL	JEOL
EBSD detector	Symmetry	Symmetry	Symmetry	Symmetry	Symmetry	Symmetry
Acquistion software (Aztec v.)	4.0	4.0	4.0	4.0	4.0	4.0
Carbon coat (<5nm)	Yes	Yes	Yes	Yes	Yes	Yes
Acc. Voltage (kV)	20	20	20	20	20	20
Working distance (mm)	20	20	20	20	20	20
Tilt (degrees)	70	70	70	70	70	70

REFERENCES

Cayron, C., 2007a, ARPGE: a computer program to automatically reconstruct the parent grains from electron backscatter diffraction data: Journal of Applied Crystallography, v. 40, no. 6, p. 1183-1188.

-, 2007b, GenOVa: a computer program to generate orientational variants: Journal of Applied Crystallography, v. 40, no. 6, p. 1179-1182.

Cayron, C., Artaud, B., and Briottet, L., 2006, Reconstruction of parent grains from EBSD data: Materials Characterization, v. 57, no. 4, p. 386-401.

Cho, J.-H., Rollett, A. D., and Oh, K. H., 2005, Determination of a mean orientation in electron backscatter diffraction measurements: Metallurgical and Materials Transactions A, v. 36, no. 12, p. 3427-3438.

Christian, J. W., and Mahajan, S., 1995, Deformation twinning: Progress in Materials Science, v. 39, no. 1–2, p. 1-157.

Erickson, T. M., Cavosie, A. J., Pearce, M. A., Timms, N. E., and Reddy, S. M., 2016, Empirical constraints on shock features in monazite using shocked zircon inclusions: Geology, v. 44, no. 8, p. 635-638.

Erickson, T. M., Pearce, M. A., Taylor, R. J. M., Timms, N. E., Clark, C., Reddy, S. M., and Buick, I. S., 2015, Deformed monazite yields high-temperature tectonic ages: Geology, v. 43, no. 5, p. 383-386.

Ni, Y., Hughes, J. M., and Mariano, A. N., 1995, Crystal chemistry of the monazite and xenotime structures: American Mineralogist, v. 80, no. 1, p. 21-26.

Schärer, U., and Deutsch, A., 1990, Isotope systematics and shock-wave metamorphism: II. U-Pb and Rb-Sr in naturally shocked rocks; the Haughton Impact Structure, Canada: Geochimica et Cosmochimica Acta, v. 54, no. 12, p. 3435-3447.

Stöffler, D., 1971, Progressive metamorphism and classification of shocked and brecciated crystalline rocks at impact craters: Journal of Geophysical Research, v. 76, no. 23, p. 5541-5551.

Timms, N. E., Erickson, T. M., Zanetti, M. R., Pearce, M. A., Cayron, C., Cavosie, A. J., Reddy, S. M., Wittmann, A., and Carpenter, P. K., 2017, Cubic zirconia in >2370 °C impact melt records Earth's hottest crust: Earth and Planetary Science Letters, v. 477, p. 52-58.

von Engelhardt, W., Stöffler, D., and Schneider, W., 1969, Petrologische Untersuchungen im Ries: Geologica Bavarica, v. 61, p. 229-295.

White, L. F., Darling, J. R., Moser, D. E., Cayron, C., Barker, I., Dunlop, J., and Tait, K. T., 2018, Baddeleyite as a widespread and sensitive indicator of meteorite bombardment in planetary crusts: Geology, v. 46, no. 8, p. 719-722.

Ries 604 monazite 14

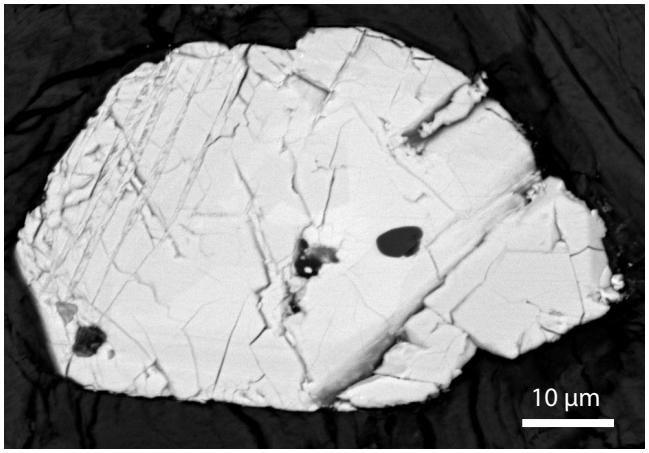

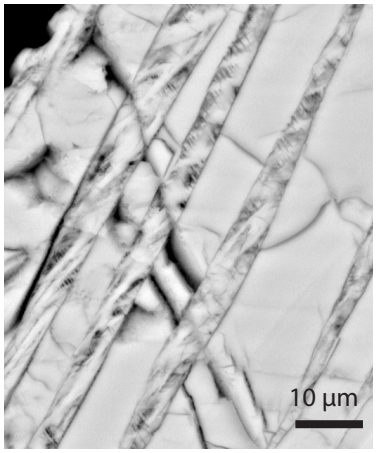

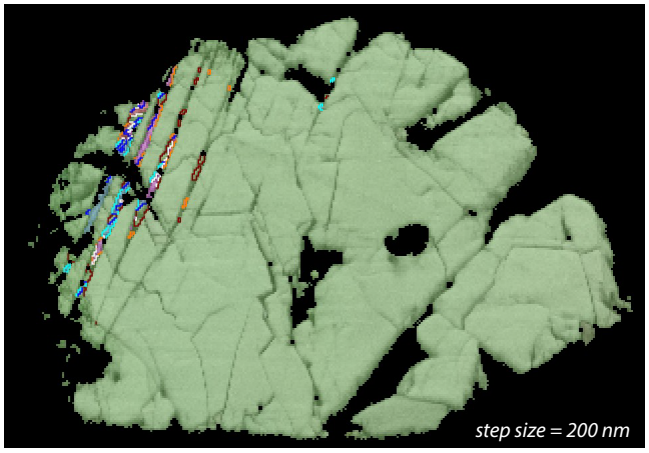

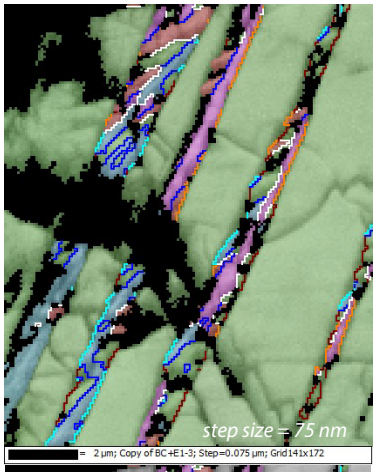

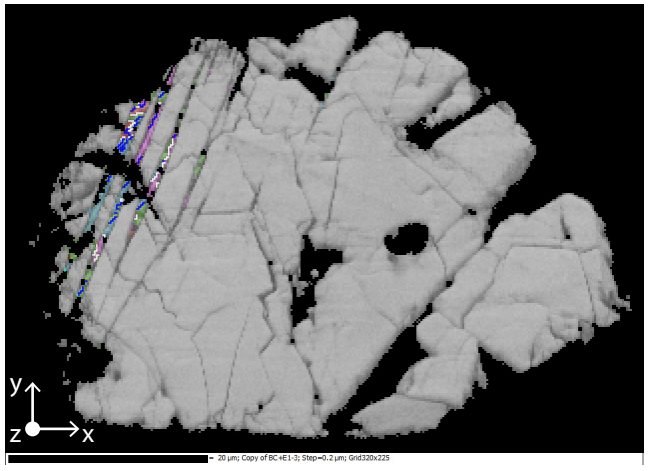

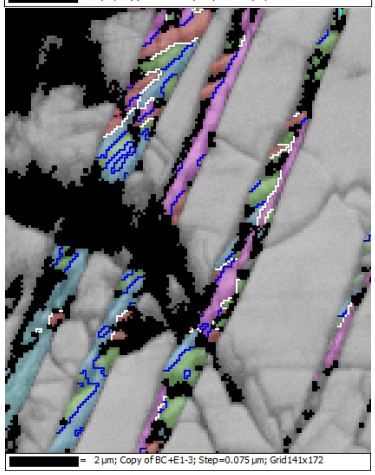

180° <100> 180° <101> 180° <001> 180° <301> 90° <301>

12° <010> 90° <401> 0° 180° 0° 180° 0° 360°

sample space

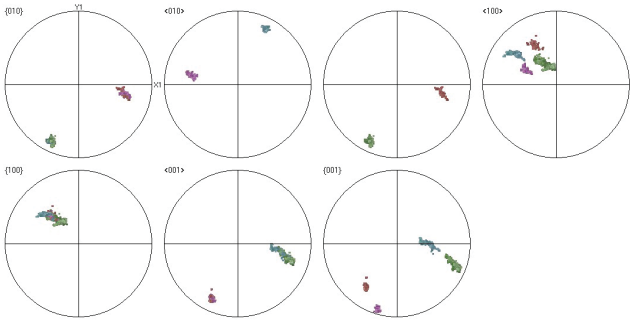

crystal space

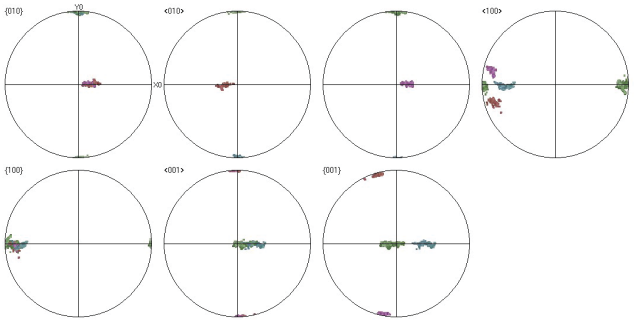

Ries 604 monazite 15

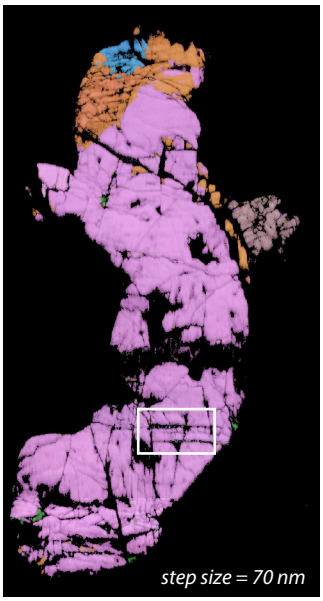

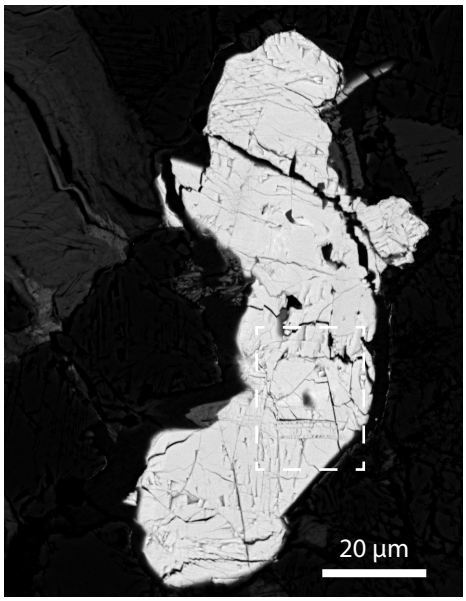

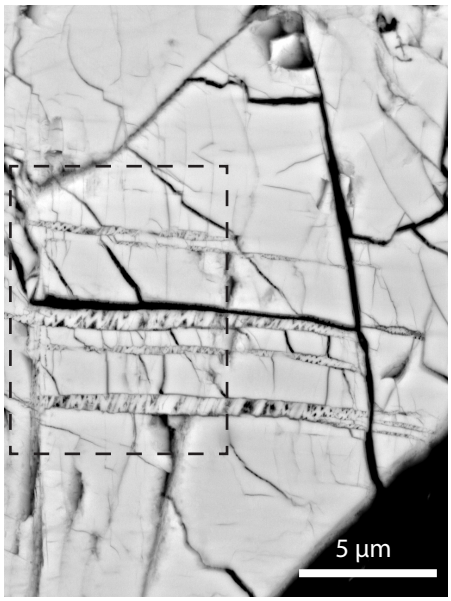

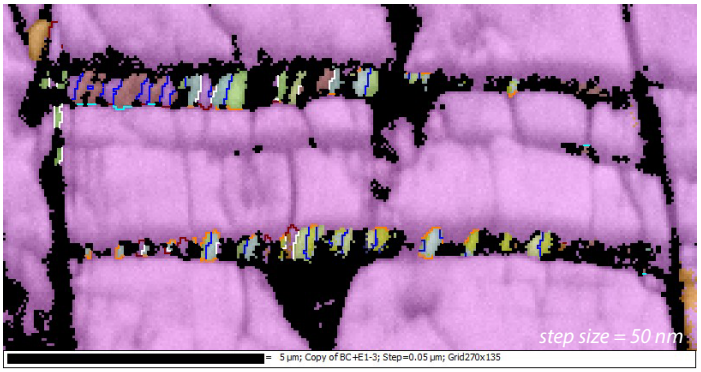

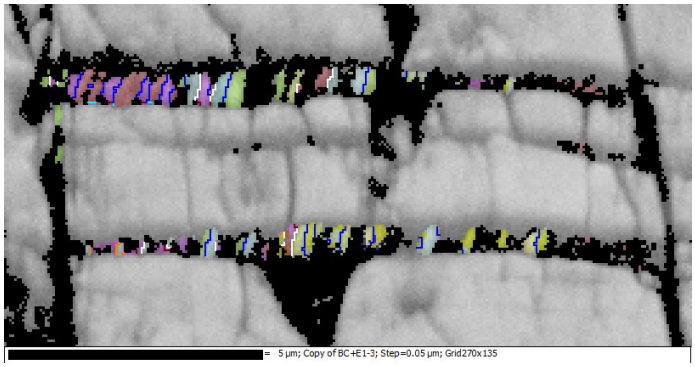

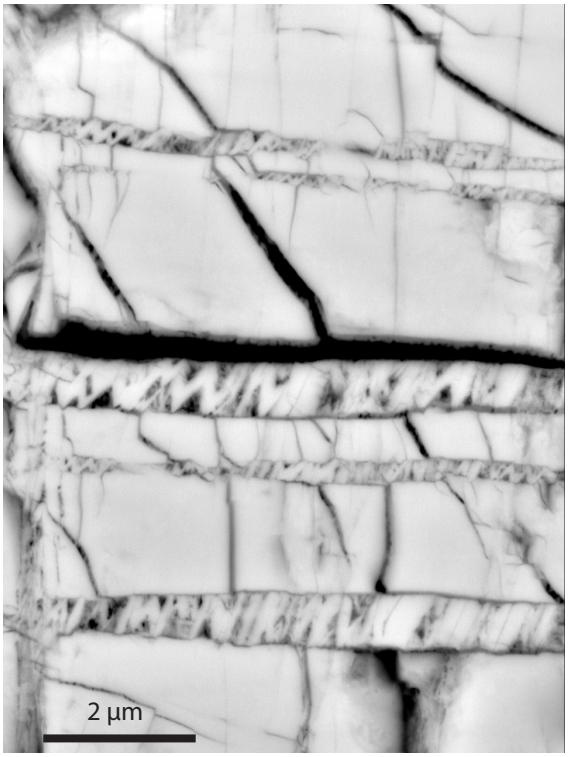

sample space

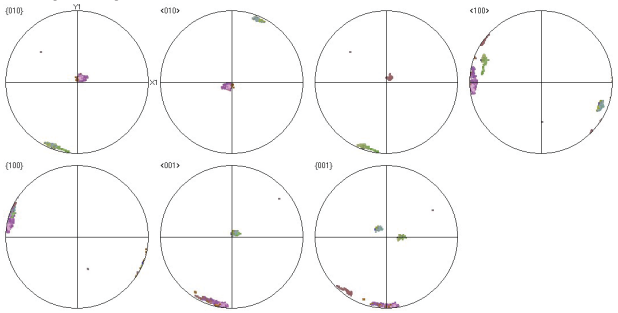

crystal space

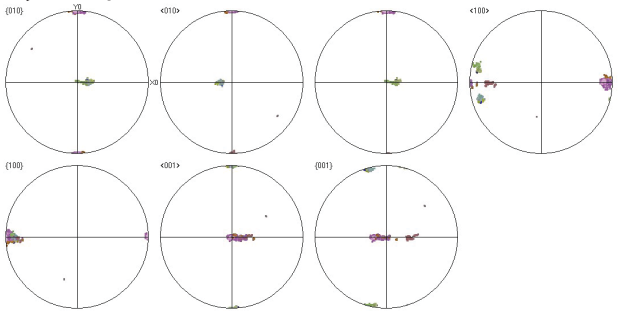

Haughton Dig9 monazite 4

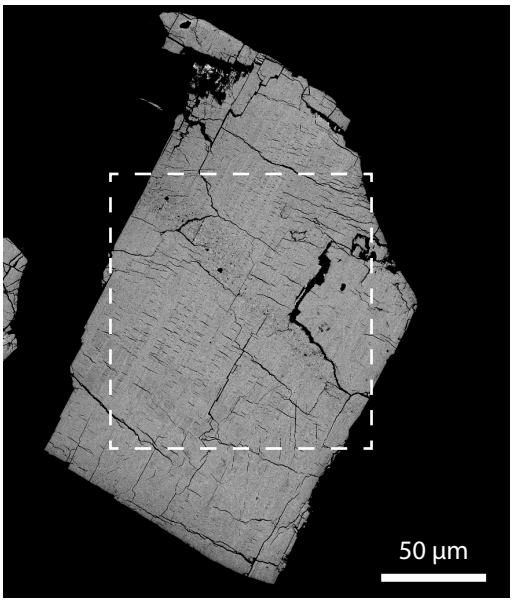

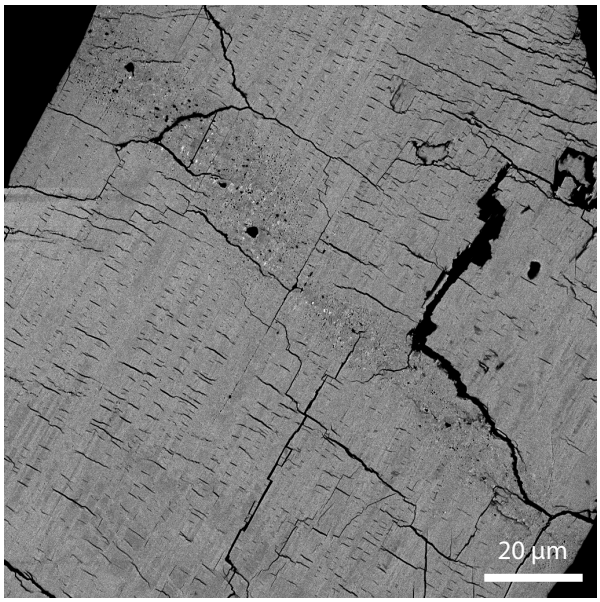

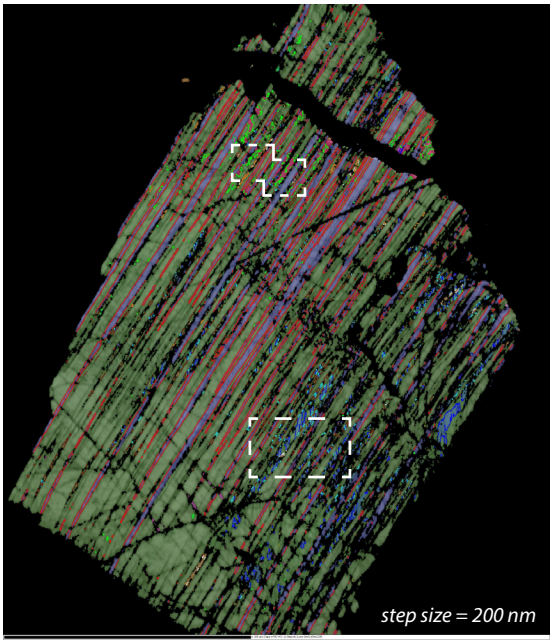

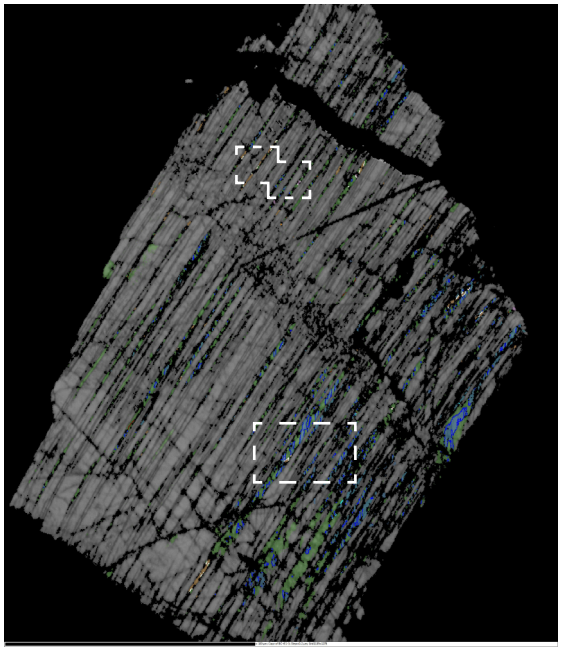

Haughton Dig9 monazite 4 cont.

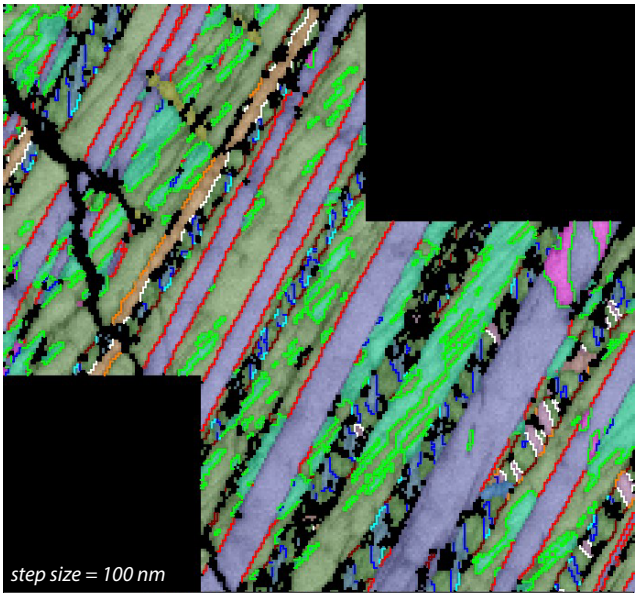

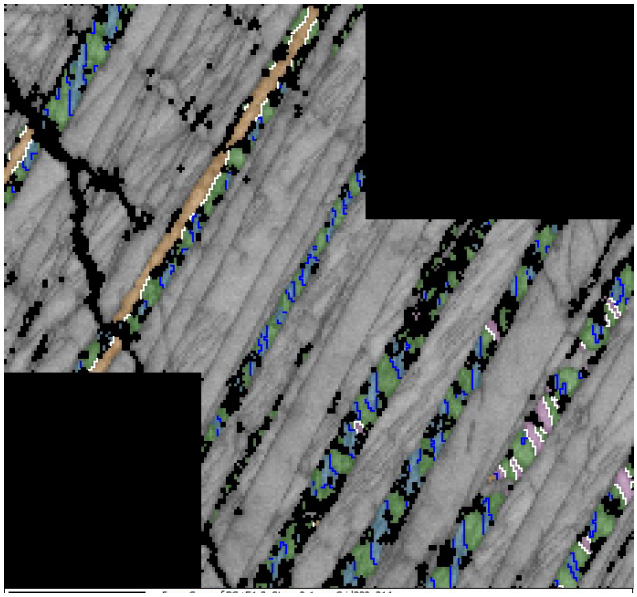

sample space

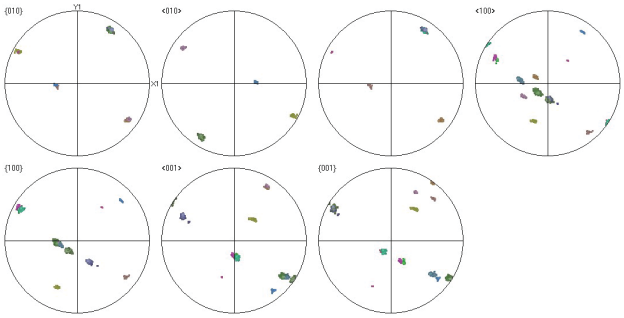

crystal space

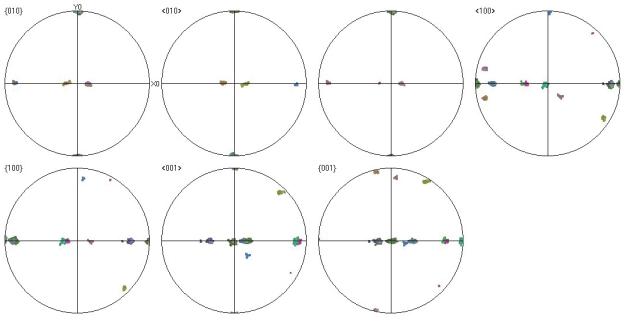

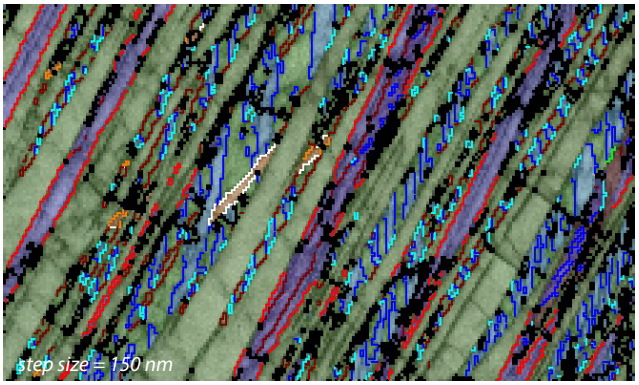

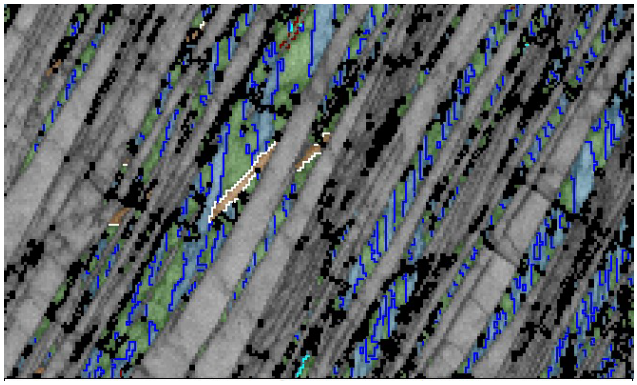

sample space

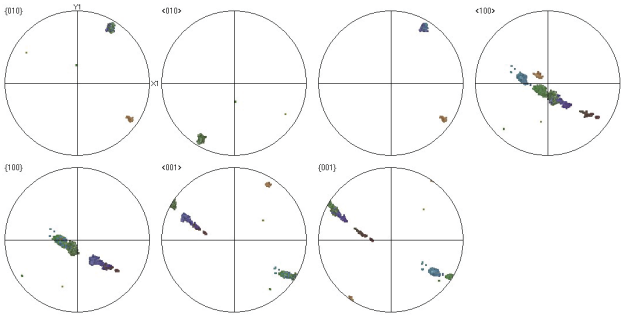

crystal space

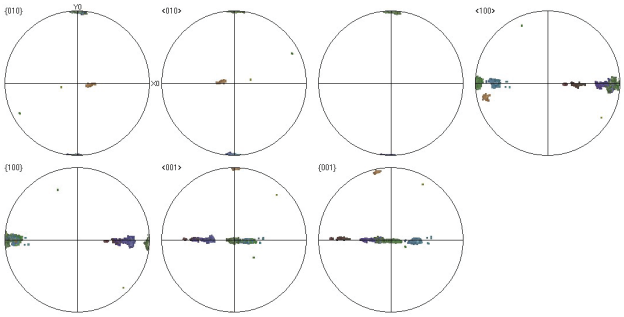

Haughton Dig9 monazite 12

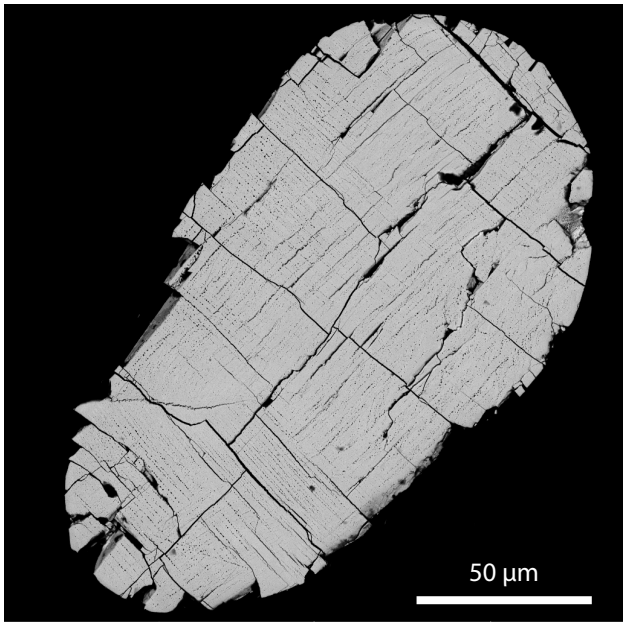

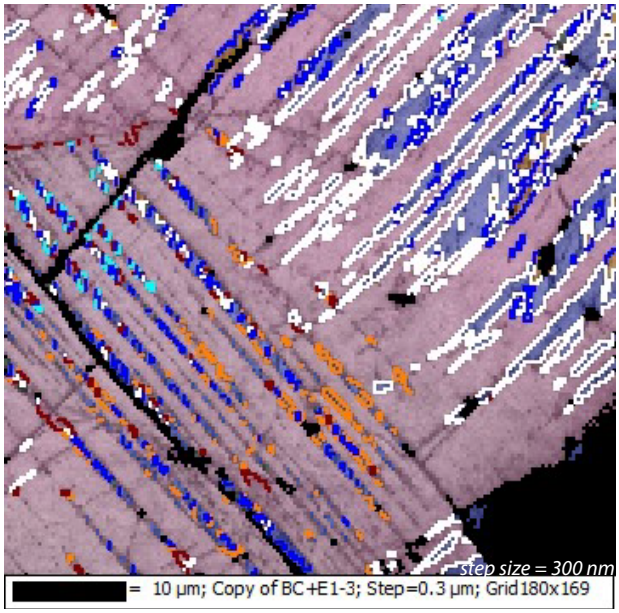

sample space

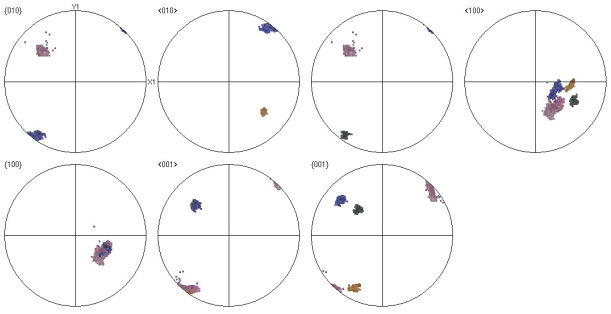

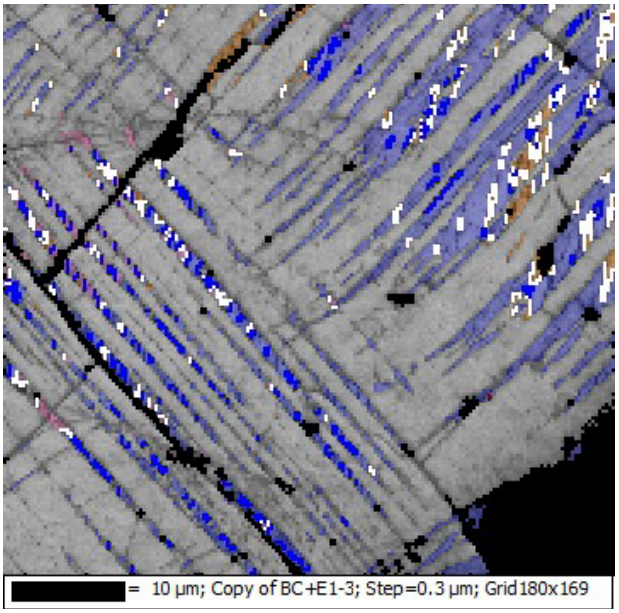

crystal space

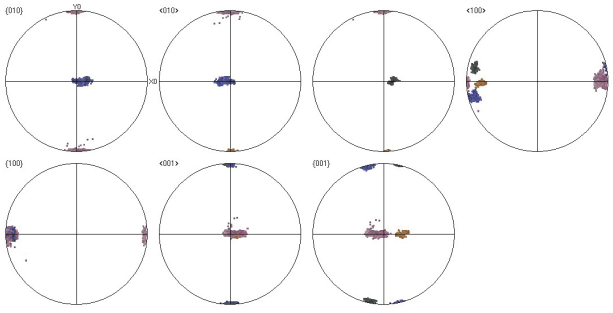

Haughton Dig9 monazite 13

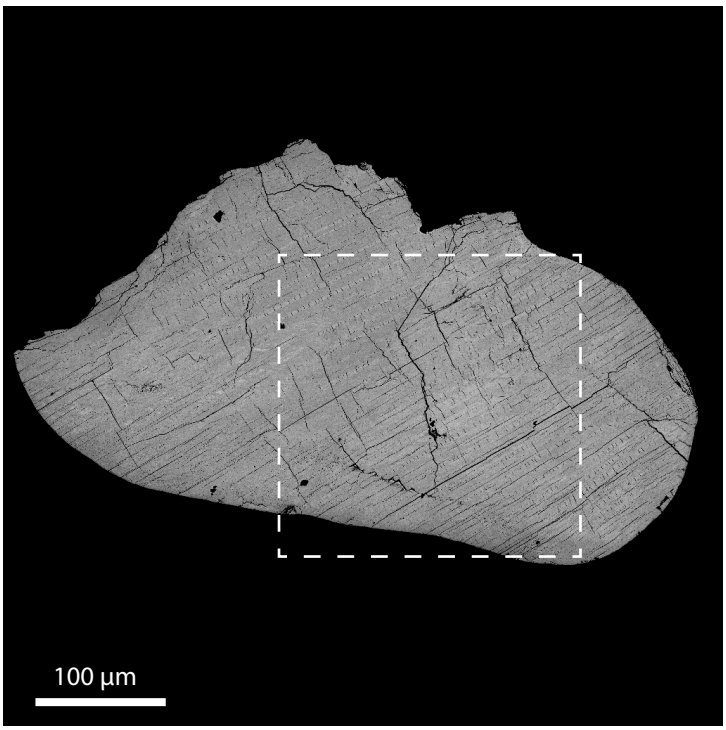

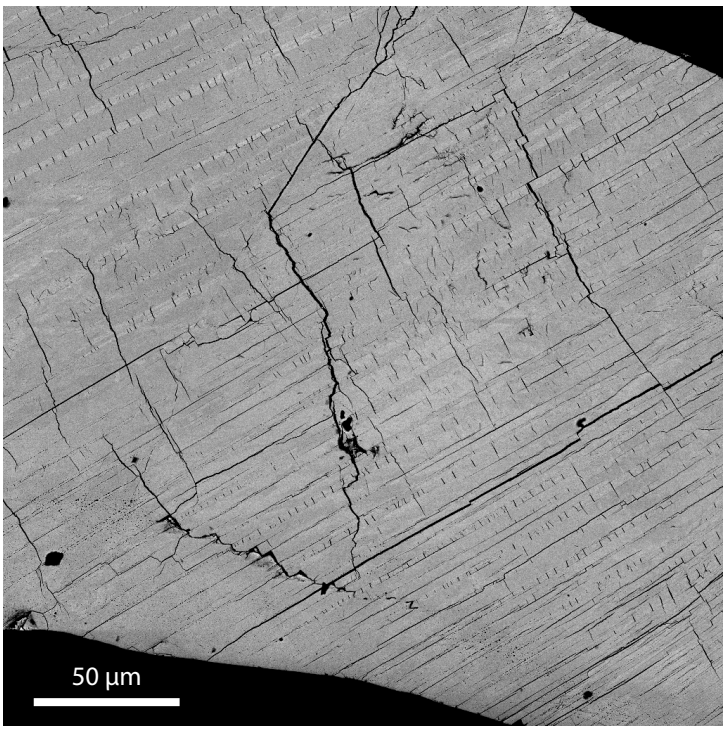

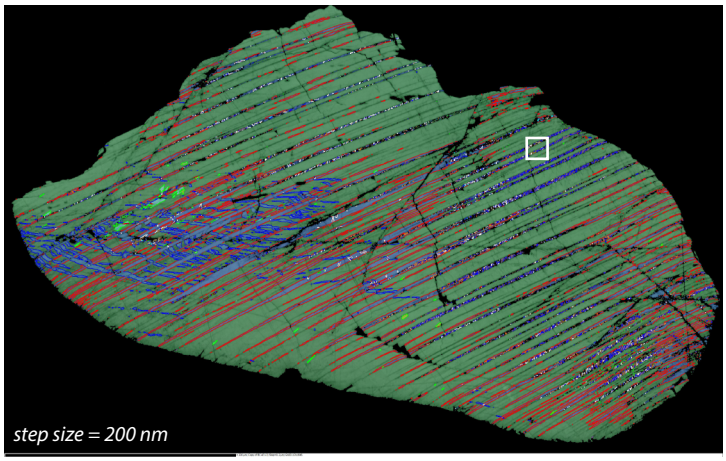

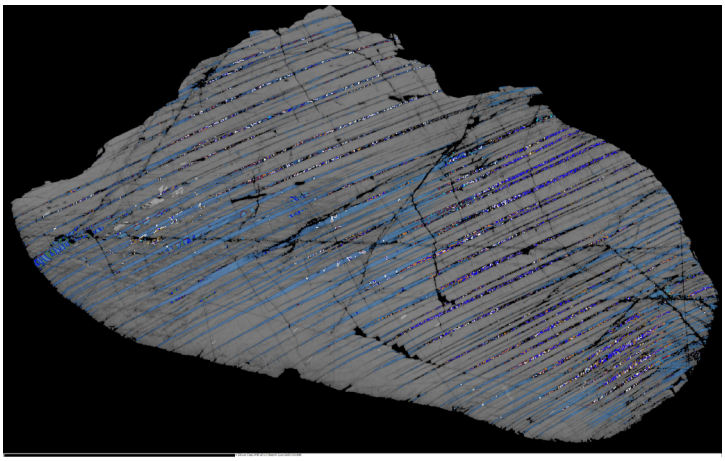

Haughton Dig9 monazite 13 cont.

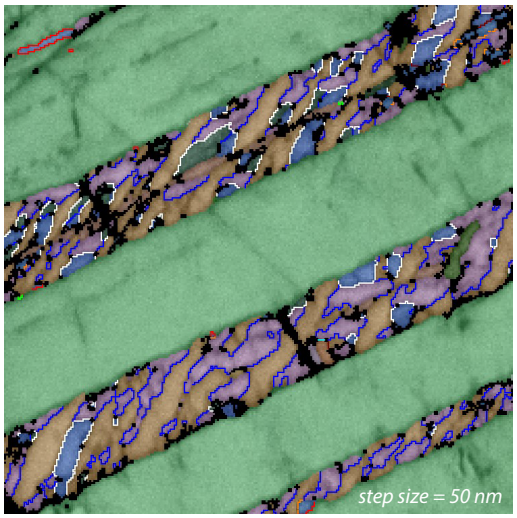

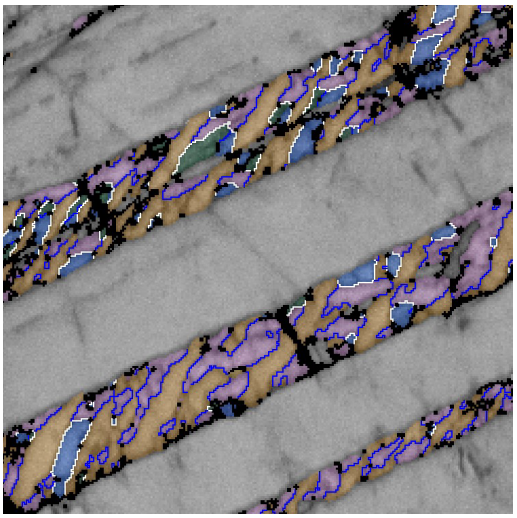

sample space

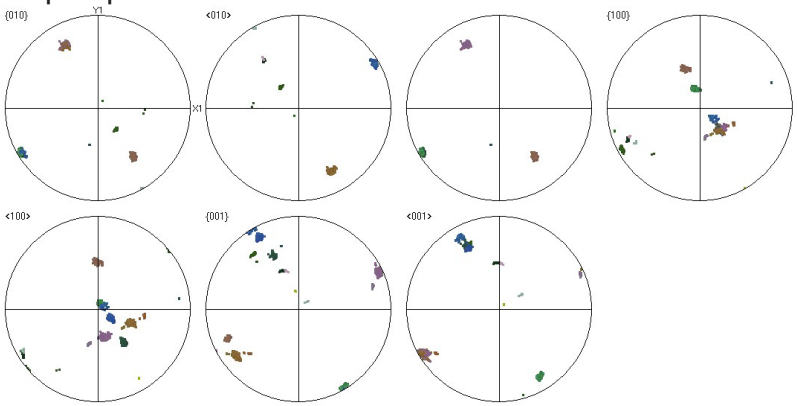

crystal space

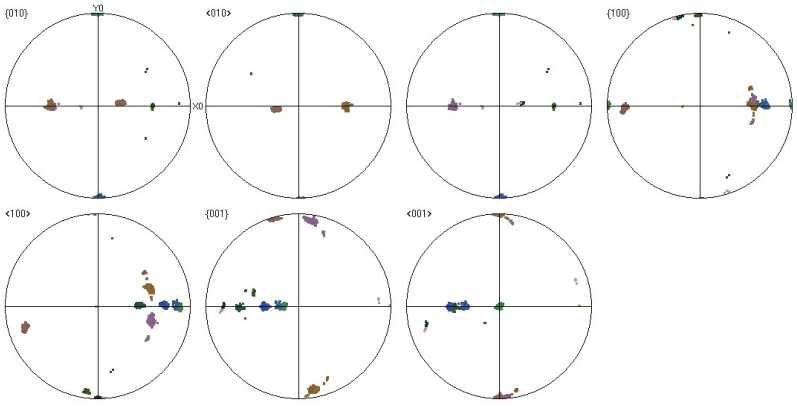

Haughton Dig9 monazite 5

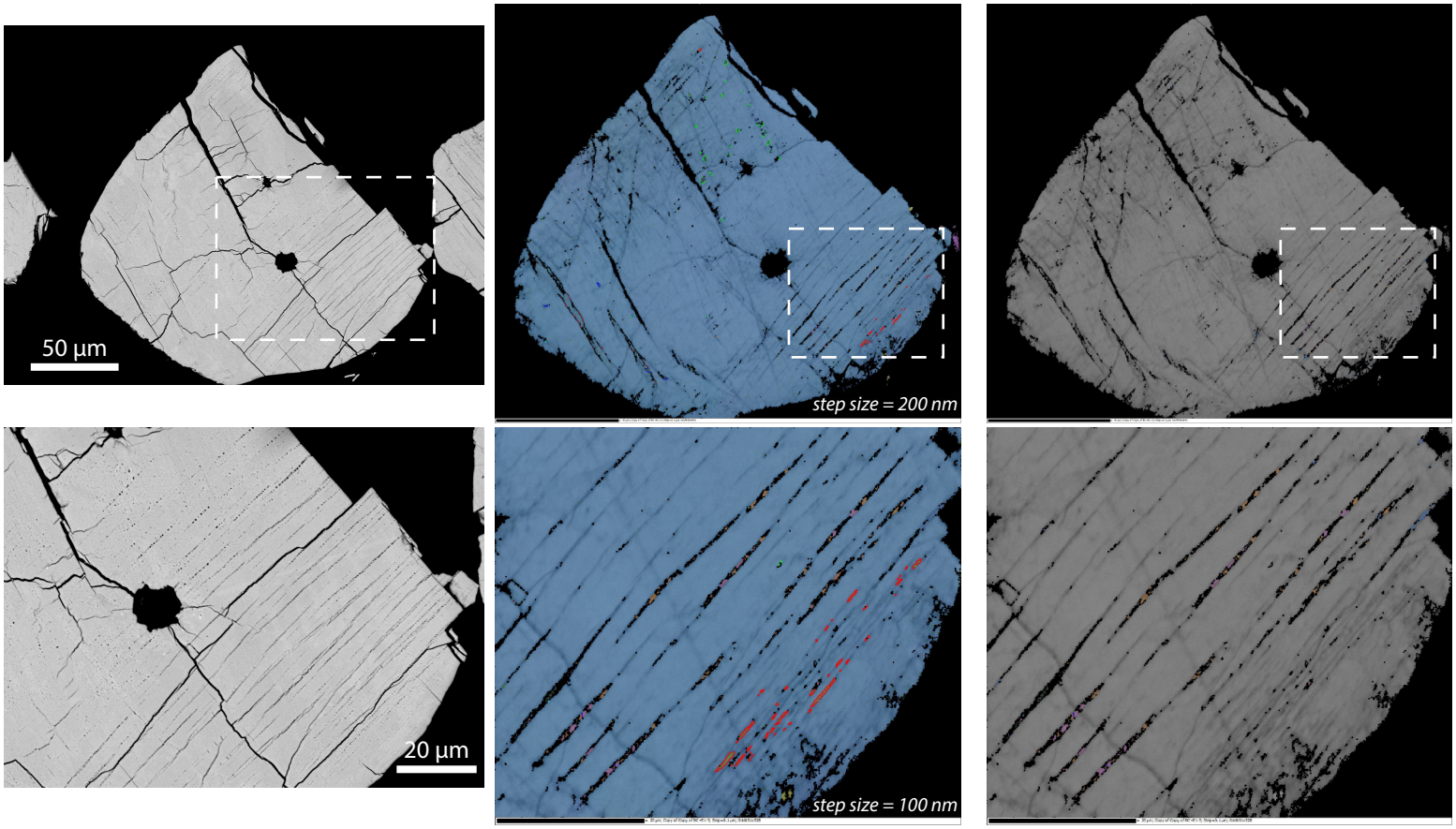

sample space

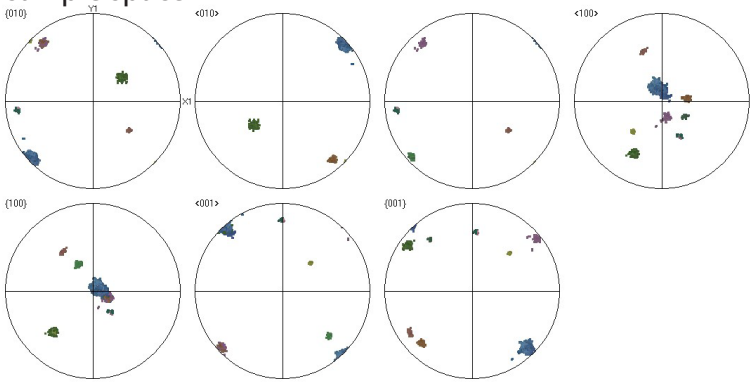

crystal space

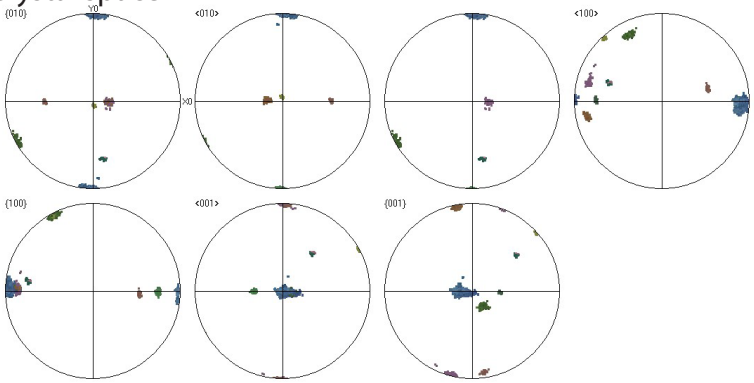

Haughton Dig9 monazite 30

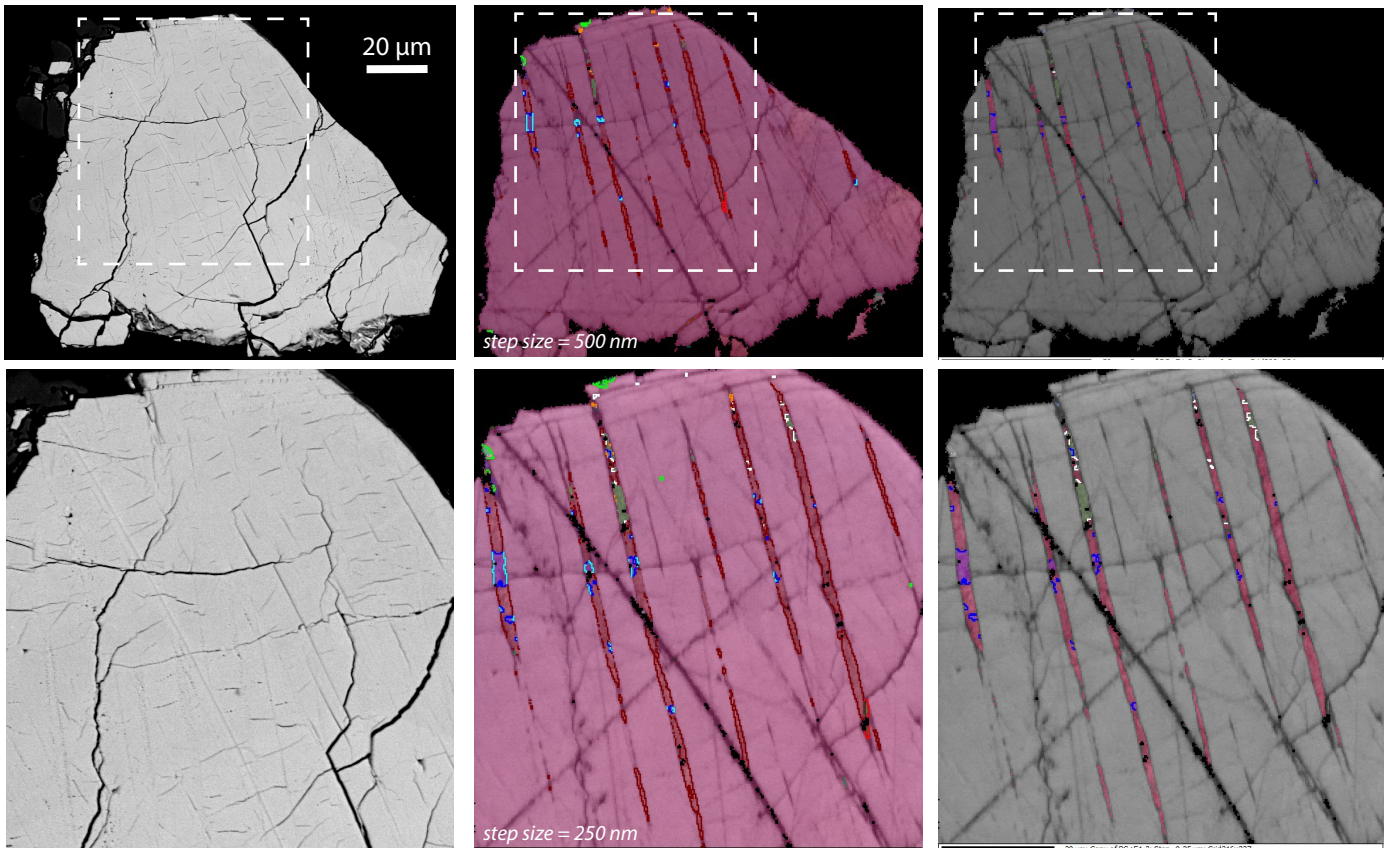

sample space

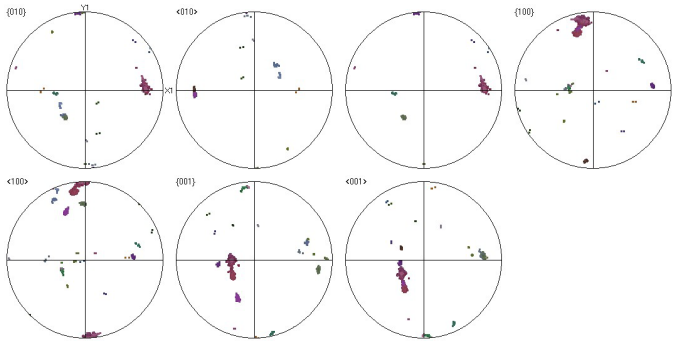

crystal space

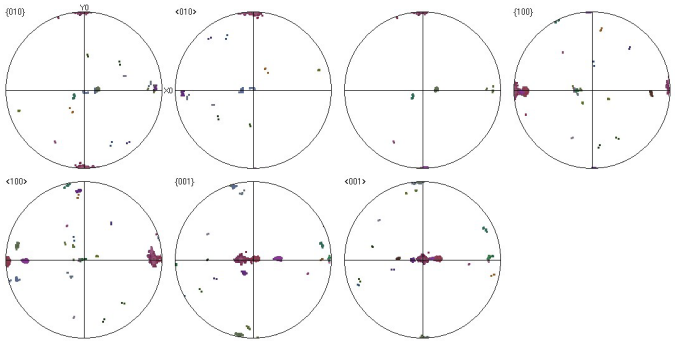

Haughton Dig9 monazite 32

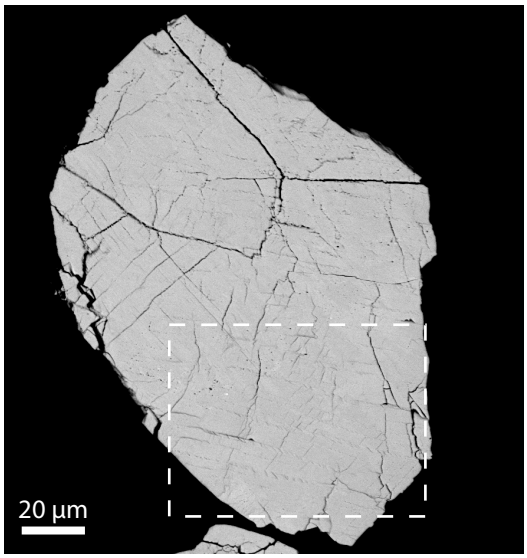

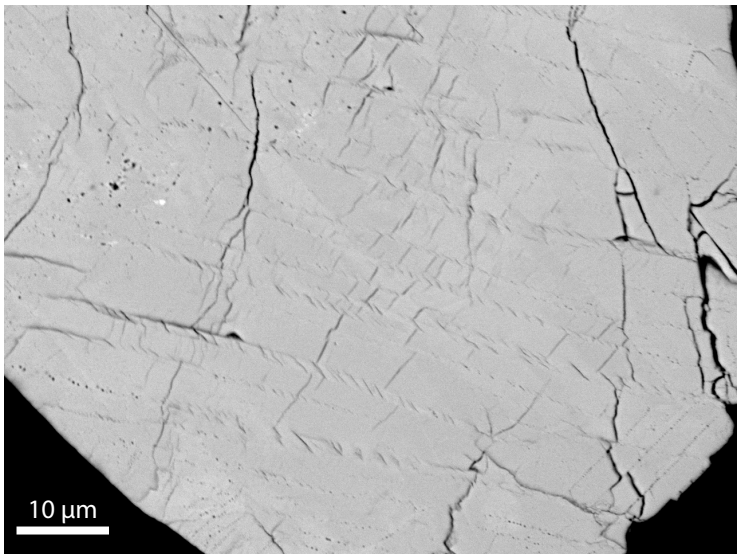

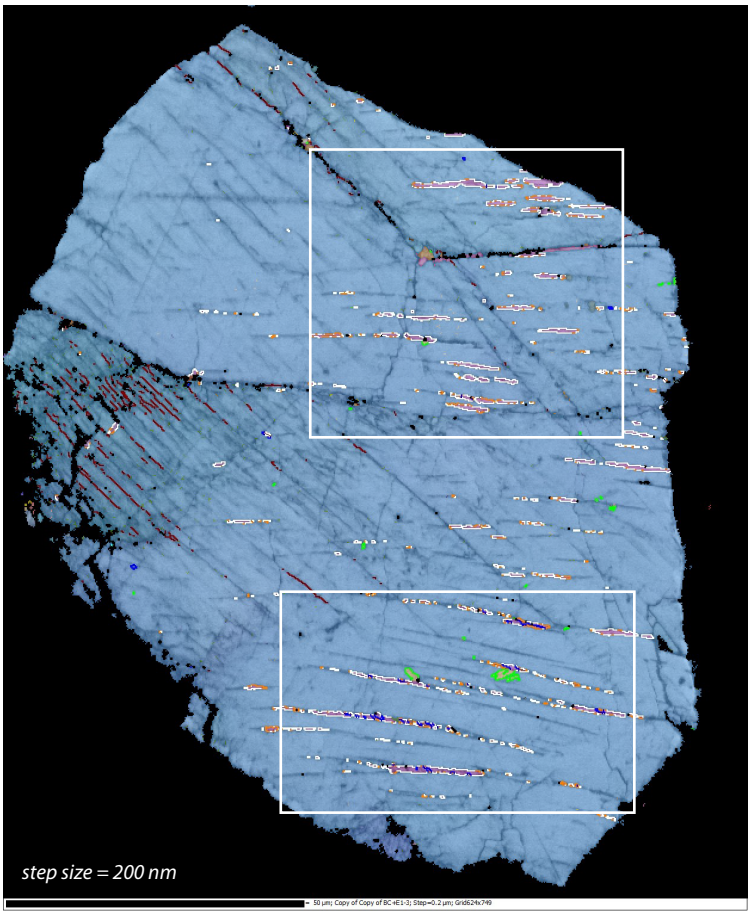

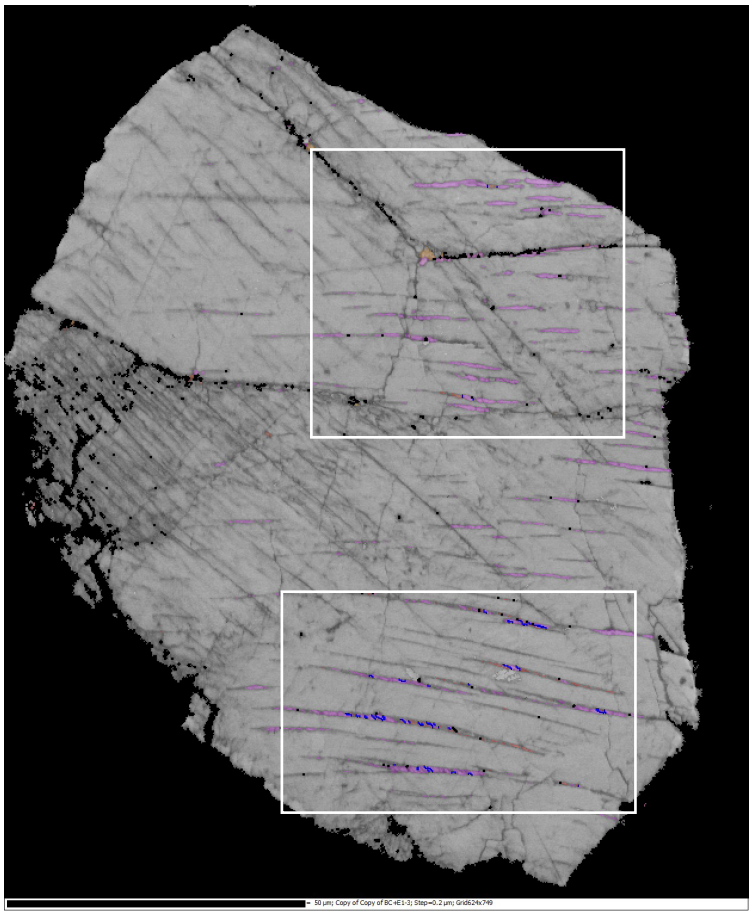

Haughton Dig9 monazite 32 continued

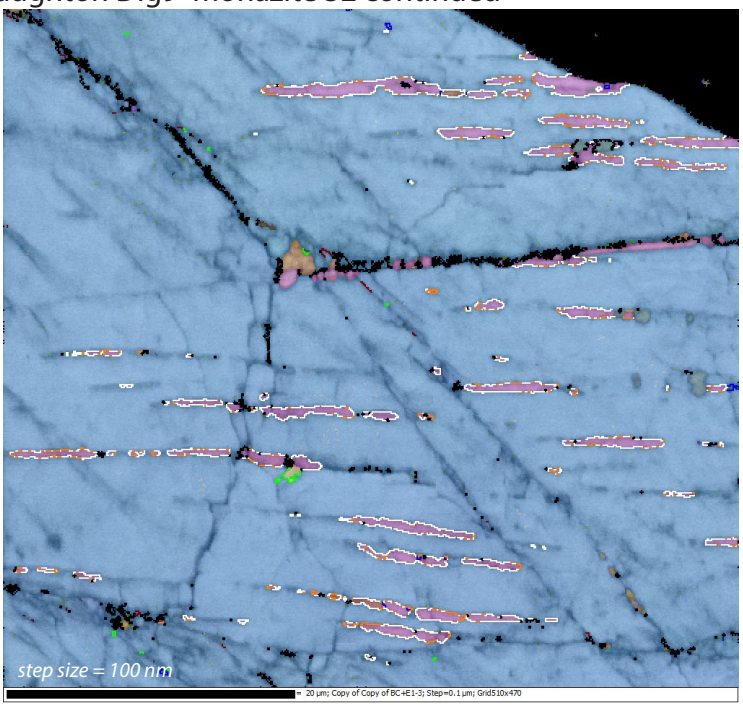

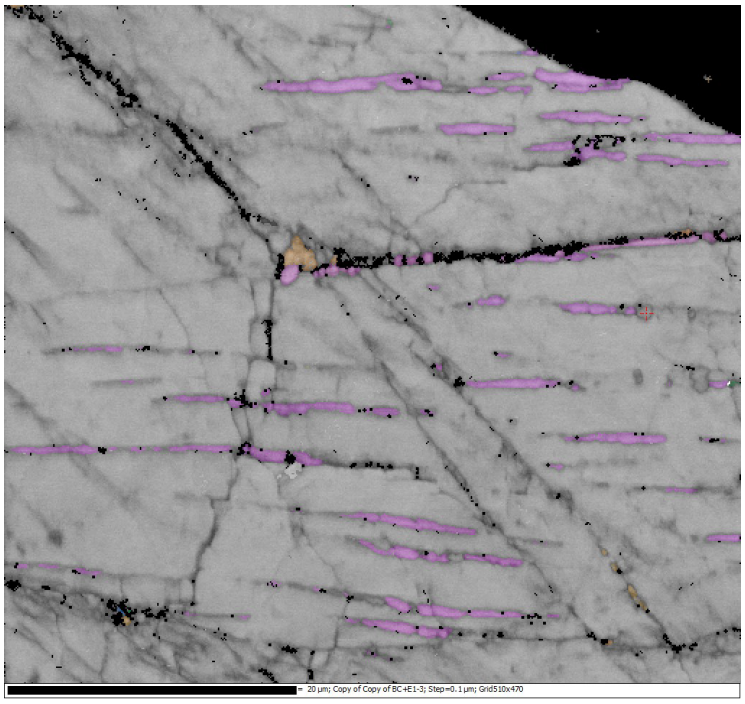

sample space

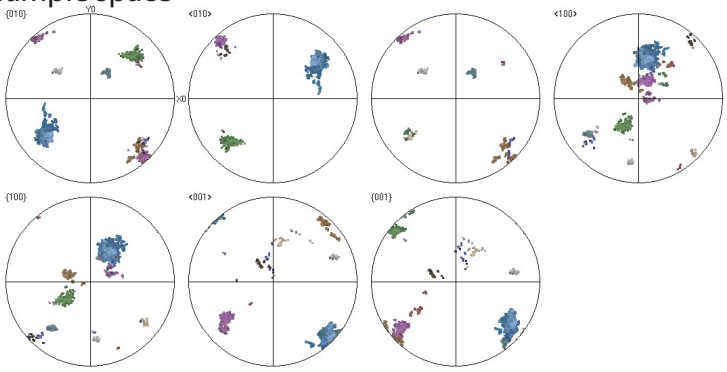

crystal space

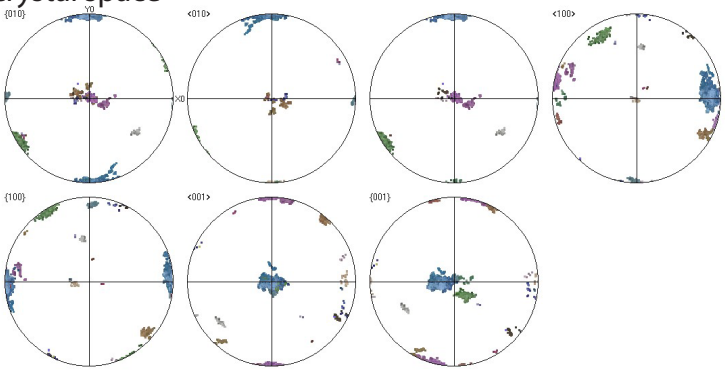

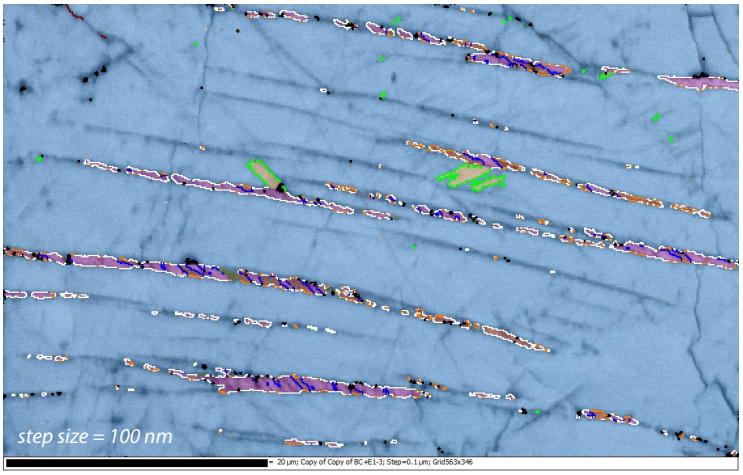

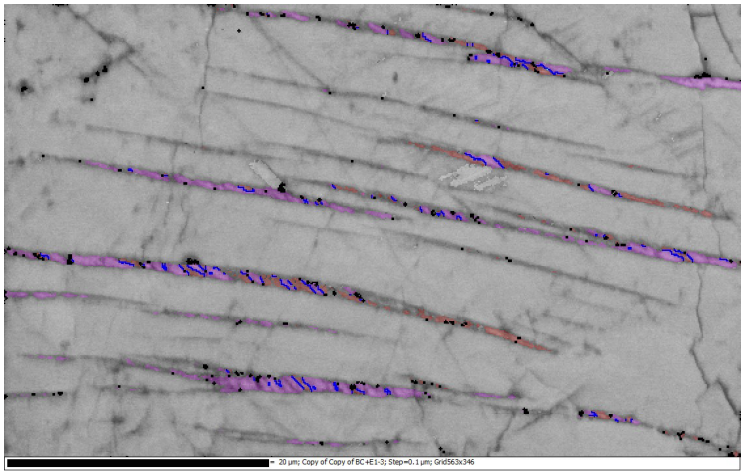

sample space

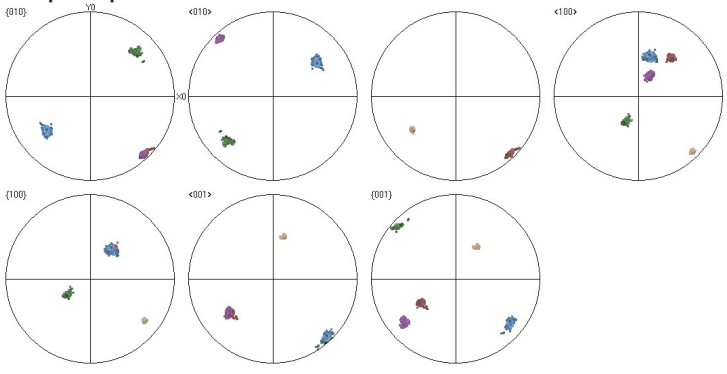

crystal space

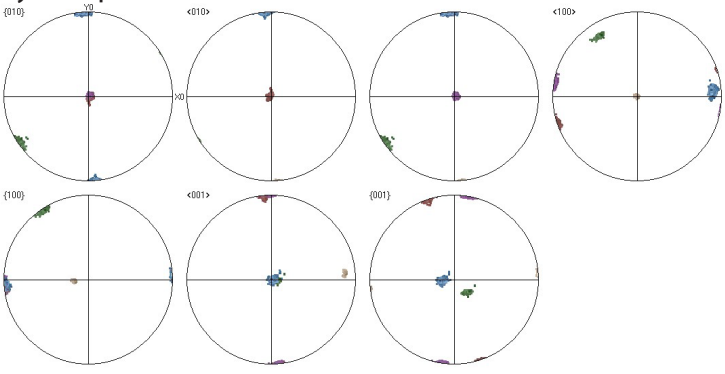

Haughton Dig9 monazite 33

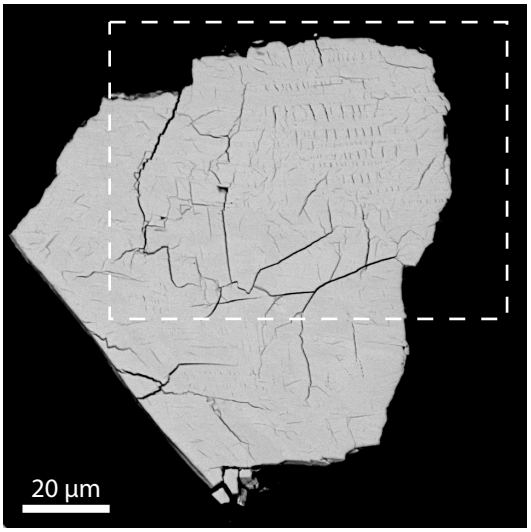

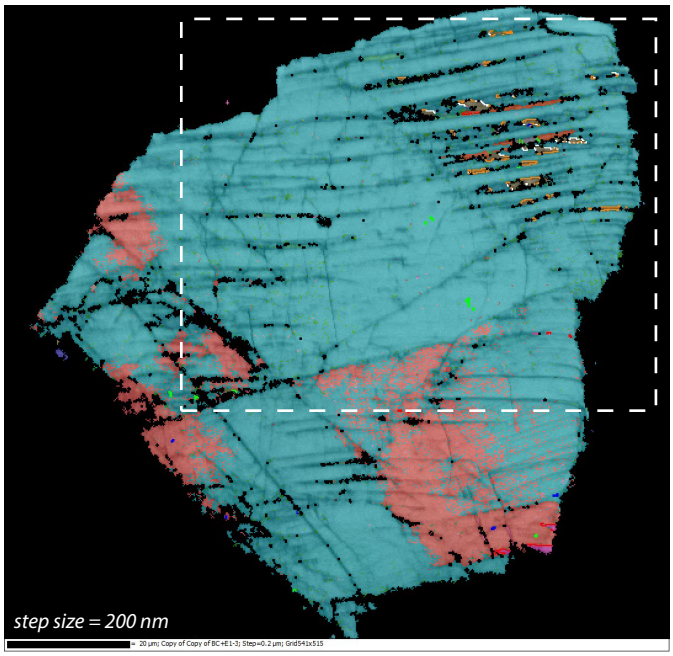

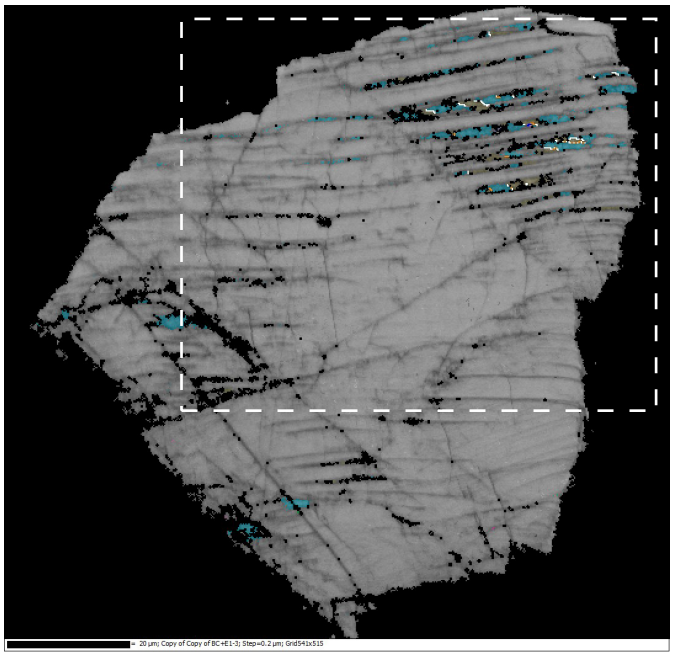

Haughton Dig9 monazite 33 continued

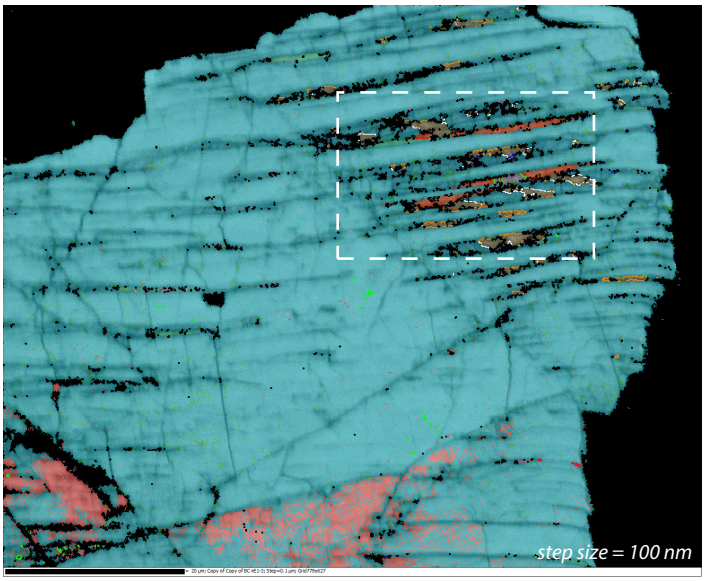

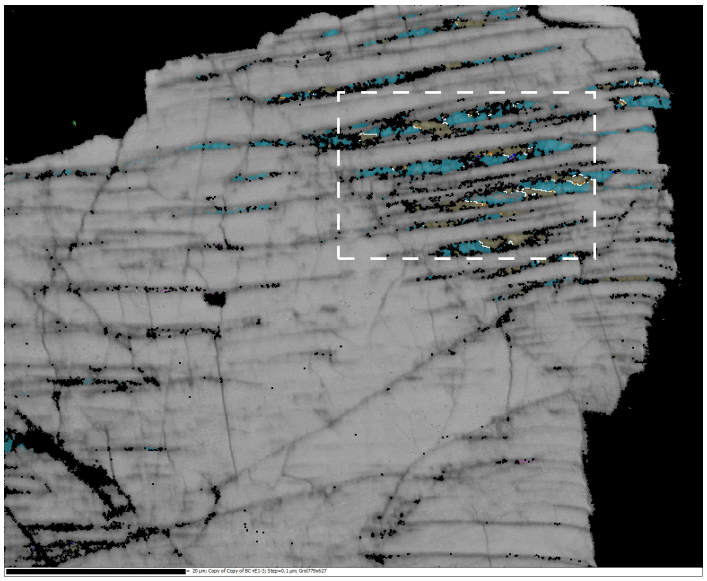

sample space

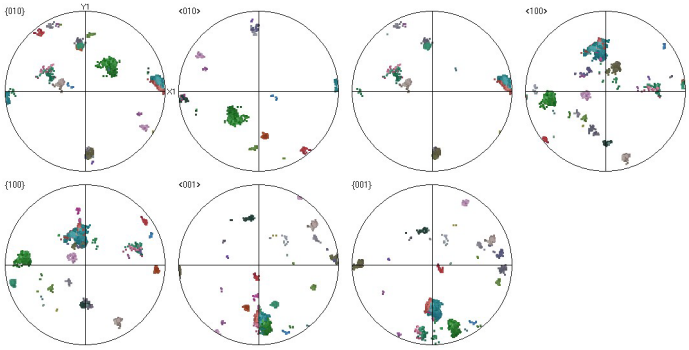

crystal space

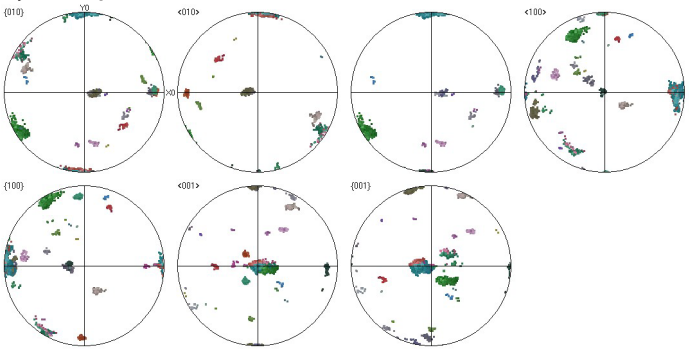

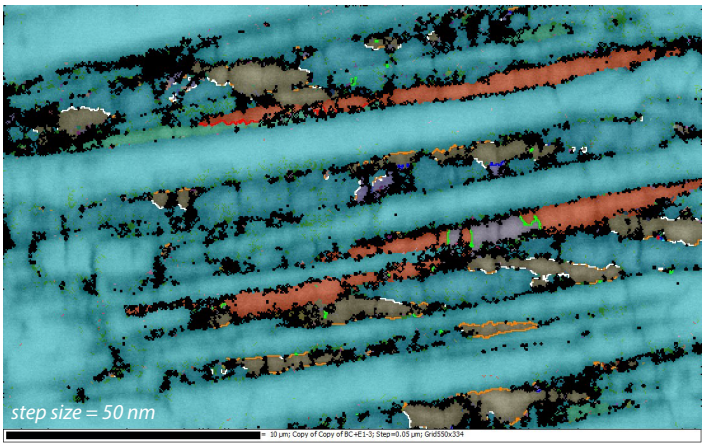

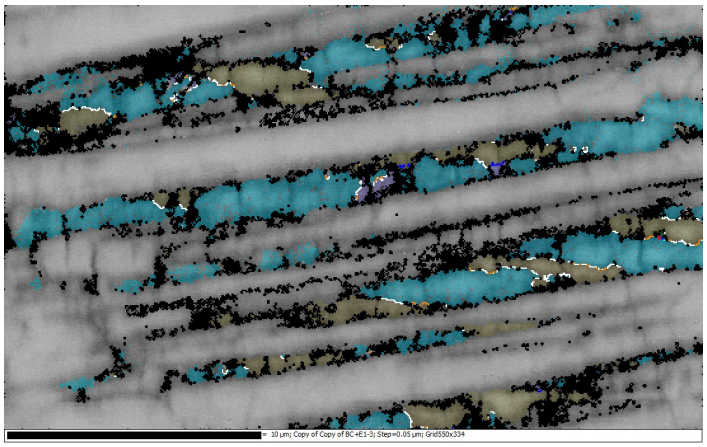

sample space

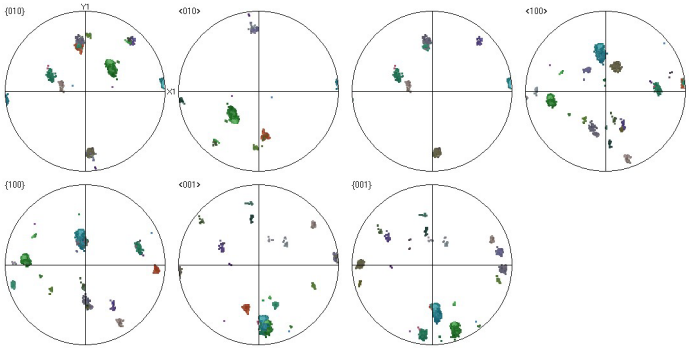

crystal space

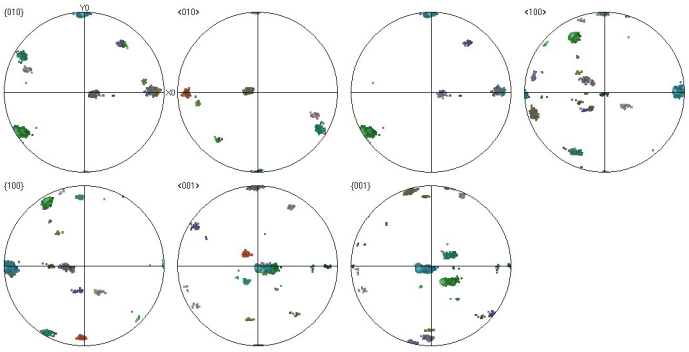

Monazte	a	b	c	α	β	γ
space group	6.7902	7.02029	6.4674	90	103.379	90

				Host				twin			Axis 1				Axis 1 Cry				Best Fit Dir			Best Fit Plane				Axis 1				Axis 1 Cry				Best Fit Dir			Best Fit Plane			
	AE color	AE color	Twin angle																																				
	host	twin	(°)	twin axis	eta 1	eta 2	eta 3	eta 1	eta 2	eta 3	Angle 1	x	y	z	a	b	c	Angle - BFD	a	b	c	Angle - BFP	a	b	c	Angle 2	x	y	z	a	b	c	Angle - BFE	a	b	c	Angle - BFF	a	b	c
Dig9 mnz5	Green	Green	18	<010>	47.32	84.98	88.1	46.9	101.8	87.4	16.8386	-0.02459	-1.72452	0.06868	-1	-65.9882	2.60985	2.42234479	0	-1	0	2.42234479	0	1	0	163.177	0.01017	1.72754	0.00364	1.64295	262.489	1	0.35842	0	1	0	0.35842	0	1	0
Dig9 mnz5	Green	Blue	180	<-30-1>	47.32	84.98	88.1	48.24	98.01	267.61	176.488	6.34188	-0.68796	-55.7187	9.79673	-1	-85.5354	6.53120343	0	0	-1	1.59969925	-1	0	3	176.584	-20.2509	0.09086	-2.30495	-236.852	1	-85.0807	1.45958	-3	0	-1	6.49844	1	0	0
Dig9 mnz5	Green	Pink	180	<-30-1>	47.32	84.98	88.1	137.69	91.83	279.82	169.503	-0.25074	1.94168	1.92337	-1	7.28663	7.59204	4.32583616	-1	4	4	3.02024783	1	-3	-3	90.42	-0.49168	-0.06445	-0.0641	-8.10771	-1	-3.04944	7.77393	-3	0	-1	7.67327	4	1	1
Dig9 mnz5	Green	Beige	90	<-30-1>	47.32	84.98	88.1	137.98	92.65	99.29	91.6787	-0.49263	-0.06467	-0.05789	-8.09568	-1	-2.93866	7.60720598	-3	0	-1	8.23221187	4	1	1	169.357	-0.22574	1.89423	1.92097	-1	7.89571	8.44875	4.88237	-1	4	4	2.21104	1	-3	-3
Dig9 mnz30	Pink	Pink	18		120.41	27.18	154.85	145.72	36.7	132.97	16.2571	-0.03592	-1.78551	0.02525	-2.10494	-98.4672	1	1.40851256	0	-1	0	1.40851256	0	1	0	163.748	0.00361	1.78657	0.00513	1	466.041	1.69594	0.20116	0	1	0	0.20116	0	1	0
Dig9 mnz30	Pink	Purple	180	<-30-1>	120.41	27.18	154.85	140.79	33.36	318.46	176.724	-2.32613	0.10544	22.3175	-23.4451	1	224.06	5.95644551	0	0	1	0.93365855	-1	0	3	179.464	-52.9164	-0.59284	-5.51541	-94.8585	-1	-33.1454	1.09854	-3	0	-1	5.98441	1	0	0
Dig9 mnz30	Pink	Green	90	<301>	120.41	27.18	154.85	94.08	115.02	153.9	91.0268	0.49221	-0.06857	0.00579	7.62836	-1	2.7365	8.00555657	3	0	1	8.17320016	4	-1	1	168.772	0.20536	1.80814	-1.81185	1	8.28507	-8.76886	5.01472	1	4	-4	2.44053	1	3	-3
Dig9 mnz30	Pink	Blue	90	<301>	120.41	27.18	154.85	95.1	114.4	336.1	172.618	0.3554	2.72259	-2.75791	1	7.20838	-7.6832	4.43000373	1	4	-4	2.4876739	1	3	-3	91.4429	0.49405	-0.04497	0.06367	11.6751	-1	4.37331	5.64144	3	0	1	8.05311	-4	0	-1
Dig9 mnz32	Green	Mustard	90	<-40-1>	48.28	77.35	58.55	129.5	120.58	76.65	89.0503	-0.49992	-0.00965	-0.00774	-55.0308	-1	-14.2399	1.2104601	-4	0	-1	1.4175433	1	0	0	178.449	-0.20035	13.1684	12.9479	-1	61.8485	65.7691	1.96466	0	1	1	2.85022	1	-4	-4
Dig9 mnz32	Green	Grey	90	<-40-1>	48.28	77.35	58.55	130.08	120.72	255.94	179.48	-0.4099	38.7694	39.0731	-1	88.9996	97.1219	2.60604524	0	1	1	2.12822523	1	-4	-4	90.4513	-0.49998	-0.0032	-0.00525	-166.094	-1	-42.1336	0.42052	-4	0	-1	0.70401	1	0	0
Dig9 mnz33	Teal	Teal	10	<010>	5.9	55.88	98.81	7.89	64.38	97.72	8.6733	-0.18637	-3.3102	0.03667	-23.8156	-398.034	-1	3.2840665	0	-1	0	3.2840665	0	1	0	171.341	0.00279	3.32104	0.01416	1	1121.97	5.43423	0.2489	0	1	0	0.2489	0	1	0
Dig9 mnz33	Teal	Purple	90	<-30-1>	5.9	55.88	98.81	101.26	82.55	243.89	173.84	-0.23122	3.29783	3.28334	-1	13.4209	14.2612	3.6084103	0	1	1	2.62123837	1	-3	-3	90.055	-0.49732	-0.03798	-0.03502	-13.9169	-1	-4.38228	4.4755	-3	0	-1	5.93046	1	0	0
Dig9 mnz33	Teal	Brown	90	<-30-1>	5.9	55.88	98.81	100.71	82.32	65.81	90.1259	-0.49602	-0.04334	-0.04568	-12.1622	-1	-4.09889	4.97711235	-3	0	-1	7.23487595	1	0	0	172.964	-0.26447	2.88857	2.87188	-1	10.2774	10.8486	4.3072	0	1	1	2.50819	1	-3	-3
Dig9 mnz33	Teal	Blue	180	<-30-1>	5.9	55.88	98.81	7.2	67.3	277.1	178.917	2.64332	0.10282	-26.323	27.3204	1	-271.254	5.73862988	0	0	-1	0.71357758	-1	0	3	179.552	64.0024	-0.60791	6.42701	111.888	-1	38.6602	0.86763	3	0	1	5.75974	1	0	0
Dig9 mnz4	Green	Green	16	<010>	57.02	93.22	74.99	53.44	108.21	75.54	15.4427	-0.04862	-1.87131	-0.14764	-1	-36.2181	-3.34473	4.7483223	0	-1	0	4.7483223	0	1	0	164.611	-0.02008	1.88399	0.00661	-10.7074	945.108	1	0.64304	0	1	0	0.64304	0	1	0
Dig9 mnz4	Green	Pink	90	<-30-1>	57.28	93.8	75.65	148.4	103.24	286.15	170.652	-0.21218	2.17779	2.16521	-1	9.65811	10.1803	4.51357296	0	1	1	2.51815192	1	-3	-3	90.3227	-0.49433	-0.05746	-0.04844	-9.14305	-1	-3.13653	6.62063	-3	0	-1	8.62752	-4	-1	0
Dig9 mnz4	Green	Blue	180	<301>	57.57	93.02	74.81	54.04	105.74	255.22	176.013	-3.34799	-0.02117	28.966	-168.102	-1	1444.68	6.5933125	0	0	1	1.53736512	-1	0	3	178.467	342.131	2.95309	39.5447	123.123	1	44.4496	1.61339	3	0	1	6.61138	1	0	0
Dig9 mnz4	Green	Beige	90	<-30-1>	57.02	93.22	74.99	148.01	104.71	106.46	90.9125	-0.49362	-0.05548	-0.05765	-9.45499	-1	-3.4251	6.56847246	-3	0	-1	8.92116993	4	1	1	170.929	-0.26141	2.2316	2.23821	-1	8.03287	8.50249	4.87881	-1	4	4	2.47005	1	-3	-3
Dig9 mnz12	Pink	Pink	16	<010>	139.17	88.1	233.69	144.46	76.9	236.14	12.7555	-0.37899	-2.16229	-0.55606	-1	-5.36856	-1.74158	5.60229529	-1	-4	-1	8.07708919	1	4	1	167.823	-0.06502	2.3691	0.04432	-2.2065	75.6489	1	1.90235	0	1	0	1.90235	0	1	0
Dig9 mnz12	Pink	Blue	90	<-30-1>	139.17	88.1	233.69	47.27	54.37	283.53	91.009	-0.49563	-0.04441	-0.04955	-11.8603	-1	-4.0927	5.13654395	-3	0	-1	7.64644472	1	0	0	172.736	-0.28006	2.77708	2.80129	-1	9.33064	9.97366	4.81885	0	1	1	2.12098	1	-3	-3
Dig9 mnz12	Pink	Beige	180	<301>	139.17	88.1	233.69	146.62	76.07	54.61	174.405	-1.81039	0.1343	14.6714	-14.3257	1	115.101	6.52157817	-1	0	4	2.04542861	1	0	-3	178.398	-27.3128	-0.46554	-3.37028	-62.3494	-1	-23.0067	2.20269	-3	0	-1	6.5724	4	0	1
Dig9 mnz12	Pink	Grey	90	<-30-1>	139.17	88.1	233.69	48.38	57.02	104.61	168.732	-0.14633	1.80632	1.80649	-1	11.6156	12.3668	4.03281526	0	1	1	2.38237699	1	-3	-3	90.7429	-0.49364	-0.06898	-0.03999	-7.60523	-1	-2.47698	7.94053	-3	0	-1	6.99185	-4	-1	0
Dig9 mnz13	Green	Green	42	<010>	30.52	106.7	94.99	28.24	64.98	97.16	41.8245	-0.0377	0.74807	-0.03413	-1	18.6728	-1.16775	3.88891016	0	1	0	3.88891016	0	1	0	138.276	0.01306	-0.75102	-0.01443	1.12973	-61.116	-1	1.48451	0	-1	0	1.48451	0	1	0
Dig9 mnz13	Green	Pink	95	<-4-11>	30.52	106.7	94.99	120.04	83.05	245.98	153.17	-0.29552	-0.76064	-0.74921	-1	-2.42197	-2.83249	4.63507419	-1	-3	-3	4.85831456	1	4	4	96.1918	-0.44454	0.15678	0.17535	-6.25282	2.07499	1	6.22561	-4	1	1	1.21316	3	-1	-1
Dig9 mnz13	Green	Beige	95	<3-10>	30.52	106.7	94.99	119.47	84.21	66.31	97.1626	-0.44725	0.16841	0.15985	-8.19081	2.90209	1	5.95568462	-3	1	0	1.88380947	3	-1	-1	150.973	-0.25319	-0.70418	-0.70844	-1	-2.61706	-3.10091	4.62114	-1	-3	-4	5.71151	1	4	4
Dig9 mnz13	Green	Blue	180	<-10-3>	30.52	106.7	94.99	27.15	66.73	275.24	176.454	235.21	0.83578	644.393	299.081	1	909.586	0.28443963	1	0	3	5.71082986	1	0	4	178.34	-192.752	-0.07478	70.3567	-2739.27	-1	355.746	5.71044	-4	0	1	0.27653	3	0	-1
Dig9 mnz13 (twin)	blue	blue	13	<010>	24.1	78.61	276.56	23.8	66.7	276.4	11.916	0.21522	-2.41145	0.05061	2.06986	-21.8225	1	5.23851529	0	-1	0	5.23851529	0	1	0	168.134	0.0053	2.4315	-0.02255	1	431.441	-4.10106	0.54593	0	1	0	0.54593	0	1	0
Dig9 mnz13 (twin)	blue	green	180	<301>	24.1	78.61	276.56	22.9	67.8	97	179.909	-29.7228	-0.36554	312.403	-86.4135	-1	906.706	5.43532321	0	0	1	0.3843737	1	0	-3	179.867	213.66	0.17098	20.3281	1328	1	451.704	0.38128	3	0	1	5.43511	1	0	0
Dig9 mnz13 (twin)	blue	beige	90	<301>	24.1	78.61	276.56	114.5	83.7	66.4	171.076	0.2358	2.25685	-2.28935	1	9.00591	-9.67366	5.01869192	0	1	-1	1.98990942	1	3	-3	91.4616	0.49459	-0.05434	0.05094	9.67299	-1	3.36779	6.29101	3	0	1	8.56424	1	0	0
Dig9 mnz13 (twin)	blue	pink	90	<-30-1>	24.1	78.61	276.56	117	81.5	246.2	91.5446	0.49449	-0.0627	0.04157	8.38203	-1	2.7562	7.20504221	3	0	1	7.66718674	4	-1	0	169.694	0.16711	1.95723	-1.98785	1	11.0211	-11.9075	4.42013	0	1	-1	1.92186	1	3	-3
Ries604 mnz14	Green	Green	15	<010>	73.19	115.58	107.7	78.18	127.76	110.04	12.8968	-0.01554	-2.23955	0.05119	-1	-135.633	3.12227	1.36836029	0	-1	0	1.36836029	0	1	0	167.107	0.00579	2.24081	0.00176	1.80839	658.87	1	0.15464	0	1	0	0.15464	0	1	0
Ries604 mnz14	Green	Blue	180	<-30-1>	73.19	115.58	107.7	77.75	126.33	290.57	178.438	5.58817	0.08697	55.82	-68.2863	1	680.124	5.71755479	0	0	1	0.66643331	1	0	-3	178.82	-160.461	-0.71867	-16.0639	-237.282	-1	-81.9128	0.70812	-3	0	-1	5.72255	1	0	0
Ries604 mnz14	Green	Pink	90	<-30-1>	73.19	115.58	107.7	155.76	72.69	310.47	169.509	-0.22009	1.95413	1.91661	-1	8.35476	8.65191	4.93333718	0	1	1	3.0241481	1	-3	-3	89.7495	-0.49255	-0.06479	-0.05656	-8.07928	-1	-2.91056	7.59283	-3	0	-1	8.345	4	1	1
Ries604 mnz14	Green	Orange	90	<-30-1>	73.19	115.58	107.7	155.1	72.25	129.1	91.4697	-0.49439	-0.04594	-0.0603	-11.4375	-1	-4.20381	5.60011314	-3	0	-1	8.42357969	-4	0	-1	172.458	-0.32961	2.66462	2.70228	-1	7.6069	8.13096	4.70618	-1	4	4	2.30252	1	-3	-3
Ries604 mnz15	Pink	Pink	15	<010>	170.64	84.46	356.22	155.16	81.59	357.79	15.6321	0.24282	-1.83922	0.03796	2.48368	-17.702	1	7.14568169	1	-4	0	7.45018532	1	-4	0	164.506	0.00526	1.87144	-0.03362	1	335.102	-6.29108	1.04159	0	1	0	1.04159	0	1	0
Ries604 mnz15	Pink	Green	90	<-30-1>	170.64	84.46	356.22	124.12	171.52	143.18	174.998	-0.41543	4.02619	4.06222	-1	9.11955	9.74481	4.90107389	0	1	1	2.13129398	1	-3	-3	90.916	-0.49654	-0.03062	-0.05078	-17.2353	-1	-5.98781	3.59625	-3	0	-1	6.80984	1	0	0
Ries604 mnz15	Pink	Blue	90	<-30-1>	170.64	84.46	356.22	148.12	174.83	348.31	91.4345	-0.49578	-0.03867	-0.05352	-13.6261	-1	-4.81308	4.56930089	-3	0	-1	7.58598684	1	0	0	173.655	-0.3471	3.16347	3.2153	-1	8.57593	9.21863	5.22112	0	1	1	1.99557	1	-3	-3
Ries604 mnz15	Pink	Brown	180	<-30-1>	170.64	84.46	356.22	158.77	82.8	177.46	179.919	36.4223	3.07212	-350.346	12.5995	1	-120.729	5.95612982	0	0	-1	1.0109535	-1	0	3	179.005	28.5123	-0.02035	2.96416	1489.3	-1	519.981	0.87977	3	0	1	5.93534	1	0	0